HYDRONAUTICS, incorporated
research in hydrodynamics

Research, consulting, and advanced engineering in the fields of NAVAL and INDUSTRIAL HYDRODYNAMICS. Offices and Laboratory in the Washington, D. C., area: 200 Monroe Street, Rockville, Md.

TECHNICAL REPORT 001-11

THE DESIGN OF TWO DIMENSIONAL LOW DRAG, BASE-VENTED STRUTS

by

S. E. Starley
and
V. E. Johnson, Jr.

March 1962

Prepared Under

Bureau of Ships
Department of the Navy
Contract Number NObs-78396
Index Number S-F 013 02 01

HYDRONAUTICS, Incorporated

TABLE OF CONTENTS

	Page
Abstract	i
Symbols	ii
List of Figures	iv
List of Tables	v
INTRODUCTION	1
THEORY	3
A. PARENT FORMS	10
1. Parabolic Strut	10
2. Plate Generated Strut	11
B. SPECIFIC LOW DRAG STRUT SHAPES	14
1. Perturbation Vorticity Distributions	
a. Fourier Series Pressure Distribution	15
(1) One Term Modified Parabolic Struts	17
(2) One Term Plate Generated Struts	20
b. "Roof Top" Pressure Distributions	23
(1) "Roof Top" Modified Parabolic Struts	26
(2) "Roof Top" Plate Generated Struts	28
C. SELECTION OF A BASE VENTED STRUT DESIGN FOR OPERATION AT ZERO BASE CAVITATION NUMBER	29
D. THE EFFECT OF FINITE CAVITATION NUMBER	30
E. THE EFFECT OF FRICTIONAL RESISTANCE ON STRUT DESIGN	34
COMPARISON OF THEORY WITH EXPERIMENT	35
CONCLUDING REMARKS	38
REFERENCES	

ABSTRACT

Linearized cavity flow theory is used to determine the shape and drag of a series of base-vented strut sections having a prescribed chordwise pressure distribution. Stagnation pressure at the nose of the strut is generated by two methods: (1) a flat plate normal to the flow at zero cavitation number, and (2) a parabolic-type nose singularity. The chordwise pressure distributions were specified in the "equivalent airfoil plane" to be either in the form of a sine series or a symmetrical flat "roof top". Numerical calculations were carried out for a series of struts derived by combining the various perturbation flows with the two types of stagnation regions to determine the strut shape, section modulus, minimum pressure coefficient and cavity drag coefficient.

Comparison of experimental and theoretical results and the effects of finite base cavitation number and frictional resistance are discussed. Charts for determining the coordinates of the optimum strut for a given design problem are presented.

SYMBOLS

a - chordwise location of break in pressure distribution of the "roof top" perturbation in hydrofoil plane

$\bar{a}$ - same as a, but in airfoil plane

A_n - coefficients in Fourier expansions

c - chord length

C_D - $= \dfrac{D}{\frac{1}{2}\rho U_\infty^2}$

C_{D_b} - $= \dfrac{D}{\frac{1}{2}\rho U_\infty^2 t_b}$

$\bar{C}_L$ - $= \dfrac{L}{\frac{1}{2}\rho U_\infty^2 C}$

C_p - $= \dfrac{p-p_\infty}{\frac{1}{2}\rho U_\infty^2}$

$K(\alpha,\phi)$ - complete elliptic integral of the first kind

$E(\alpha,\phi)$ - complete elliptic integral of the second kind

ℓ - cavity length expressed in chords

m - trailing edge slope

p - local pressure

p_∞ - static pressure in the free stream

q - dynamic pressure = $\frac{1}{2}\rho U_\infty^2$

t_b - strut base thickness

u - the x component of the perturbation velocity in the hydrofoil plane, expressed as a fraction of U_∞

$\bar{u}$ - the x component of the perturbation velocity in the airfoil plane, expressed as a fraction of U_∞

SYMBOLS (Continued)

v	-	the y-component of the perturbation velocity in the hydrofoil plane, expressed as a fraction of U_∞
$\bar{v}$	-	the y-component of the perturbation velocity in the airfoil plane, expressed as a fraction of U_∞
x	-	a space coordinate in the hydrofoil plane, parallel to U_∞; its origin coincides with the leading edge, expressed as a fraction of chord length
y	-	vertical space coordinate in the hydrofoil plane, expressed as a fraction of chord length
α	-	$= \frac{\pi}{2}$
θ	-	a dummy variable in the airfoil plane, defined by $\theta = \cos^{-1}(-\xi)$
η	-	imaginary coordinate in the airfoil plane
ξ	-	real coordinate in the airfoil plane
ρ	-	mass density of incompressible fluid
σ	-	cavitation number $= (p_\infty - p_c)/\frac{1}{2}\rho U_\infty^2$
σ_i	-	incipient cavitation number $= C_{p\ min}$
σ_b	-	cavitation number based on base cavity pressure
ϕ	-	$= \sin^{-1} \frac{1}{\sqrt{\ell+1}}$
$\bar{\Omega}$	-	vorticity strength in the airfoil plane

Subscripts

o	-	one term perturbation
a	-	roof top perturbation
0	-	trailing edge
p	-	parent body
c	-	cavity

LIST OF FIGURES

Figure No.

1. Base Vented Strut - Supercavitating Hydrofoil Configuration
2. Linearization of Base Vented Strut Problem
3. Chordwise Pressure Distribution on Parabolic Struts
4. Drag Coefficient of Parabolic Struts (σ_b=0)
5. Definition Sketch for the Plate Generated Form
6. Exact and Approximate Solution for Cavity Drag Coefficient vs. Thickness Ratio for the Plate Generated Form
7. Shape Comparison of Plate Generated Form and Parabola, t_b=.20
8. Vorticity Distributions in the Airfoil Plane
9. One Term Chordwise Pressure Distribution
10. One Term Modified Parabolic Struts
11. One Term Modified Parabolic Struts With Finite Cavity Drag
12. Comparison of One Term Struts, σ_i= .10
13. "Roof Top" Pressure Distributions
14. "Roof Top" Modified Parabolic Struts, Zero Cavity Drag
15. "Roof Top" Modified Parabolic Struts With Finite Cavity Drag, a= .9
16. Comparison of "Roof Top" Struts, a= .8, σ_i= .1
17. Cavity Drag Coefficient vs. Base Cavitation Number For Various Struts
18. Cavity Length vs. Base Cavitation Number for Various Struts
19. Strut With Base Annex
20. Parabolic Strut Drag Coefficient vs. Froude Number Parameter, t_b= .167
21. Parabolic Strut Drag Coefficient vs. Froude Number Parameter, t_b= .21

LIST OF TABLES

Table No.

I.a Plate Generated Parent Forms, t_b=.04, .06, .08, .10

I.b Plate Generated Parent Forms, t_b=.12, .14, .16, .18

I.c Plate Generated Parent Forms, t_b=.20, .22, .24, .26

I.d Plate Generated Parent Forms, t_b=.28, .30, .32, .34

II.a "Roof Top" Perturbation, a= 0, .1, .2, .3

II.b "Roof Top" Perturbation, a= .4, .5, .6, .7

II.c "Roof Top" Perturbation, a= .8, .9, 1.0

HYDRONAUTICS, Incorporated

THE DESIGN OF TWO DIMENSIONAL LOW DRAG, BASE-VENTED STRUTS

INTRODUCTION

Hydrofoil sections currently envisioned for application in high speed hydrofoil craft are either supercavitating sections with an upper surface cavity vented to the atmosphere or base cavitating sections with the base cavity vented to the atmosphere. In either type of foil the simplest and most practical method of providing ventilation air is to support the hydrofoil with one or more base ventilated surface piercing struts as illustrated in Figure 1. The cavity created behind such blunt based struts forms a natural air passage from the atmosphere to the hydrofoil region requiring ventilation air. The satisfactory operation of base-vented struts has been demonstrated in many experiments, see for example, References 1 and 2.

Considerable effort has been expended during recent years to successfully maximize the hydrodynamic efficiency of supercavitating hydrofoils (References 3 - 6). The overall optimization of the hydrodynamic efficiency of a strut-hydrofoil combination obviously requires that similar studies directed toward minimizing the strut drag be carried out. Since the strut thickness and area in some designs may be comparable to the thickness and area of the hydrofoil, very significant improvements in performance can be achieved by minimizing the strut contribution to the total drag. In References 7 and 8 it is pointed out that relatively thick base vented struts having zero cavity drag are theoretically possible; however such struts necessarily produce reduced pressure over their chord and thus, for high speed operation, there exists the possibility of vapor cavitation over the chord.

In a given design problem the strut is usually required to house some shafting or other device of fixed dimensions and must additionally be structurally adequate to support the loads on the system. Consequently the base-vented strut design problem may be summarized as follows: Find the strut shape having a specified section modulus which will enclose a given configuration with the least hydrodynamic resistance without cavitating along its chord at a given design speed. Furthermore the magnitude of the drag of the strut selected must be determined for both zero and finite base cavitation numbers.

This report presents the results of an analysis which leads to the solution of the two dimensional strut design problem outlined in the preceeding paragraph and presents design charts and tables which enable the designer to select theoretically optimum struts with a minimum of additional computation. The analysis treats only the case of two dimensional struts operating at zero angle of yaw; consequently no information is obtained concerning the yaw sensitivity of base vented struts to spontaneous ventilation along one side. Nor does the analysis consider the possibility of partial ventilation of the rearward portion of the strut chord caused by too steep pressure gradients and boundary layer separation on the after portion of the strut. These aforementioned effects are not amenable to theoretical analysis and experimental investigations of these critical areas should be made to aid the designer in selecting a final strut design.

Furthermore it is recognized that three dimensional effects (free water surface and finite span) will tend to reduce the drag coefficients and incipient cavitation numbers determined from two dimensional theory. However, it is

speculated that the reduction in profile drag caused by the strut-water surface intersection is compensated for by the so-called spray drag. Furthermore, if the lower surface of the strut is attached to a hydrofoil (or pod) the hydrofoil end-plate effect will greatly diminish the three-dimensional effects in the lower region of the strut. Hence, in practical strut-hydrofoil configurations, the cavity drag is expected to be nearly identical to the cavity drag of the strut in two dimensions. In view of these remarks, struts may be designed according to the two dimensional theory developed in this report and applied directly to practical designs without consideration for three dimensional effects. Struts so designed, may be expected to have cavity drags and incipient cavitation numbers no greater than the two dimensional design values and possibly slightly less; the designs will therefore be conservative.

THEORY

Ideally, the strut design problem may be reduced to a problem in variational calculus in which the strut drag is minimized subject to constraints related to specified section modulus, thickness, and incipient cavitation number. However, the complications involved in such an elegant analysis are not warranted if adequate results may be obtained by simpler methods.

Two alternate methods of investigating the strut problem are apparent. One is to specify a general family of struts by some analytic function such as a polynomial and then to determine the significant hydrodynamic characteristics of the strut in terms of the coefficients of this polynomial. Probably the most important characteristic of the strut is its drag coefficient which may be obtained in terms of the strut shape

from the following equation which is derived by Tulin in Reference 7.

$$C_D = \frac{2}{\pi}\left[\int_0^c \frac{dy}{dx}\frac{dx}{\sqrt{c-x}}\right]^2 \qquad [1]$$

However, the analysis given in Reference 7 does not give directly the pressure distribution on the body and an unnecessarily large number of forms must be examined in order to study bodies of near optimum pressure distribution.

A more straightforward method of investigating the strut problem is to specify families of chordwise pressure distribution and to determine the characteristics of the resulting strut forms. This is the exact same method used by Tulin, Johnson, and Auslaender in References 3, 5, and 6 to study families of supercavitating hydrofoils. In fact the linearized cavity flow theory of Tulin developed in Reference 3 for lifting surfaces is particularly applicable to the strut problem when the chordwise pressure distribution is specified.

In the linear theory described in Reference 3, the absolute velocity components in the x and y directions are defined as $U_\infty + u'$, and v' respectively; where u' and v' are referred to as perturbations to the undisturbed free stream which flows with steady uniform velocity U_∞ in the x direction. The principal assumption of the linear theory is that the perturbation velocities u' and v' are small with respect to U_∞ so that higher order combinations of the velocity ratios ($\frac{u'}{U_\infty}$, and $\frac{v'}{U_\infty}$) may be neglected. Thus, the boundary condition which prescribes that the velocity vector be tangent to the body surface may be stated as $\frac{dy}{dx} = \frac{v'}{U_\infty}$ rather than the exact

relationship $\frac{dy}{dx} = \frac{v'}{U_\infty + u'}$. Similarly the pressure coefficient $C_p = \frac{p-p_\infty}{\frac{1}{2}\rho U_o^2}$, may be related in linearized theory to the perturbation velocities by the simple equation $C_p = -\frac{2u'}{U_\infty}$. It should be clear that the assumptions made in the linearized theory are valid only if the streamline slopes and local pressure coefficients are indeed small. Thus the linear theory will be applicable to the strut problem if the struts are reasonably thin. A second assumption of the linear theory follows from this restriction to thin struts - it is assumed that the boundary conditions which are prescribed on the strut or cavity walls may be satisfied on the x axis. Justification for the assumptions made in the linear theory are best made by comparing the linearized results with exact solutions or experiment. Such comparisons have been made in Reference 3, 5, and 7 where linearized results were shown to be in very good agreement with results from more exact methods. Further justification for the application of linearized cavity flow theory to the problem of low drag strut design does not seem to be required.

In order to simplify the notation in analyzing the strut problem, the perturbation velocity ratios $\frac{u'}{U_\infty}$ and $\frac{v'}{U_\infty}$ are denoted throughout the remainder of this report as simply u and v so that the linearized boundary conditions referring to streamline slopes and pressure coefficients become $\frac{dy}{dx} = v$ and $C_p = -2u$.

The strut problem is shown in the physical plane in

Figure 2a along with the appropriate linearized boundary conditions. In order to simplify the analysis the strut chord is taken as unity so that the coordinates x and y may be interpreted as non-dimensional ratios of distances to chord; that is $\frac{x}{c}$ and $\frac{y}{c}$. The base cavity is assumed to be completely vented so that the pressure within the cavity is the same as the free stream pressure and thus the pressure coefficient along the cavity streamline is zero. Since $C_p = -2u$, the boundary condition that must be satisfied along the cavity wall is simply $u=0$. Again, since $C_p = -2u$, arbitrary distributions of the pressure coefficient along the chord of the strut may be prescribed simply in terms of $u(x)$. In order to satisfy the condition of no flow through the boundary the additional condition $v = \frac{dy}{dx}$ is prescribed. In the linear theory these boundary conditions are to be satisfied on the x axis so that the strut problem becomes the simple semi-infinite slit as indicated in Figure 2b.

Following the method of Reference 3, the flow outside the slit in the physical plane may be transformed into the lower half of the ζ plane by the transformation $\zeta = -\sqrt{Z}$; the boundary conditions prescribed in the physical plane are carried over to corresponding points in the ζ plane as shown in Figure 2c. In order to distinguish the values of the perturbation velocities between the physical plane, Z, and the transformed plane, ζ, the barred symbols ($\bar{u}$, $\bar{v}$) are used in the ζ plane. Since the strut is symmetric, the pressure distribution must be identical on both sides of the strut. Thus in the transformed plane the pressure distribution will be

symmetric about the y axis as indicated in Figure 2c.

The problem indicated in Figure 2c is the well known thin airfoil problem which may be solved simply by distributing singularities (vortices) in the interval $-1 \leq \xi \leq 1$ such that the vortex strength $\Omega(\xi) = 2\bar{u}(\xi)$. The vertical velocity perturbation $\bar{v}(\xi)$ may then be obtained by summing up at the point ξ the individual vertical components induced by the vortices located at the point ξ' in the interval $-1 \leq \xi' \leq 1$. So that

$$\bar{v}(\xi) = \int_{-1}^{1} \frac{2\bar{u}(\xi')}{2\pi(\xi'-\xi)}\, d\xi' \qquad [2]$$

Hence,

$$\frac{dy}{dx}(\xi) = \bar{v}(\xi) = \frac{1}{\pi} \int_{-1}^{1} \frac{\bar{u}(\xi')}{(\xi'-\xi)}\, d\xi' \qquad [3]$$

Now the strut ordinates in the physical plane may be obtained from the following equation

$$y(x) = \int_{0}^{x} \frac{dy}{dx}(x)\, dx \qquad [4]$$

Since $\frac{dy}{dx}(x) = \frac{dy}{dx}(\xi)$ at corresponding points in the physical and transformed planes such that $x = \xi^2$, $\xi = \sqrt{x}$, and $dx = 2\xi d\xi$, Equation [4] may be written as

$$y(x) = 2 \int_{0}^{\sqrt{x}} \bar{v}(\xi)\, \xi\, d\xi \qquad [5]$$

where $\bar{v}(\xi)$ is given by Equation [3].

The drag coefficient of the strut based on the strut chord is obtained by an investigation of the pressure coefficients over the projected area normal to the stream and may be expressed as

$$C_D = -2 \int_0^1 C_p(x) \frac{dy}{dx} dx = 4 \int_0^1 u(x) \frac{dy}{dx} dx \qquad [6]$$

or in terms of the transformed problem

$$C_D = 2 \int_{-1}^{1} \bar{u}(\xi) \frac{dy}{dx}(\xi) 2\xi d\xi = 4 \int_{-1}^{1} \bar{u}(\xi)\bar{v}(\xi)\xi d\xi \qquad [7]$$

In Reference 3, the integral in Equation [7] is shown to be equivalent to

$$C_D = \frac{2}{\pi} \left[\int_{-1}^{1} \bar{u}(\xi) d\xi \right]^2 \qquad [8]$$

Since $\bar{C}_L$, the lift coefficient of the equivalent airfoil, may be written as $2 \int_{-1}^{1} \bar{u}(\xi) d\xi$, Equation [8] may be interpreted as

$$C_D = \frac{1}{2\pi} \bar{C}_L^2 \qquad [9]$$

Thus if symmetric pressure distributions are prescribed in the airfoil plane, the value of $\bar{C}_L$ may be immediately evaluated as $4 \int_0^1 C_p(\xi) d\xi$ and from Equation [9], the drag coefficient of the resulting strut is obtained.

No physical strut will exist if completely negative pressure distributions are prescribed because such pressure distributions produce negative upper surface ordinates and positive lower surface ordinates. This result is comparable to the non-physical results obtained for most low drag supercavitating foils where at the shock free entry angle the cavity streamline is given by the theory to be below the lower surface of the foil.

In the supercavitating lifting surface theory, practical foils of reasonable thickness are obtained by adding singular-like loadings near the leading edge which may be produced by angle of attack or parabolic thickness. The final foil shape may then be considered as a basic parabolic shape or flat plate

(with cavity) shape which has been perturbed by the low drag, shock free entry ordinates.

The derivation of useful strut shapes may be accomplished in a similar manner; that is, by using the ordinates given in Equation [5] as perturbations which are added to basic shapes which have singular behavior near the nose such as parabolas or wedges. It is true that strut shapes may be obtained which do not have a singular point at the nose and which do have positive thickness everywhere along the chord. Such struts would have cusped noses and positive pressures over some portion of the chord. These cusped nosed struts would not be acceptable for even small angles of yaw and were therefore not given further consideration.

The obvious base vented strut shape to be used as a parent form is that shape which initially has no negative pressures along its chord and which has a minimum drag for a given thickness or section modulus. Using the hydrodynamic comparison theorem (see Reference 9), it is shown in Reference 7 that the minimum drag basic shape described above is the profile generated by the zero cavitation number cavity behind a flat plate normal to the flow. Furthermore, it is shown in Reference 7 that the linearized approximation to this optimum shape is a parabola. Consequently the parent strut forms selected for use in the parent study were the parabola and the flat plate generated form. Before proceeding with the various perturbations which were applied to these parent forms, it is important to summarize the characteristics of these parent shapes without the perturbations.

PARENT FORMS

Parabolic Struts

If in the airfoil plane shown in Figure 2 a single vortex with a clockwise circulation and strength $\frac{\pi}{2} U_\infty t_b$ is located at the origin, a parabolic strut of base thickness t_b will be generated in the physical plane. This strut has a singular loading at the nose followed by a uniform zero pressure coefficient along its chord. The lift on the equivalent airfoil corresponding to the single vortex which generates the parabola is $\frac{\pi}{2}\rho U_\infty^2 t_b$ and the corresponding lift coefficient on the foil whose chord is 2 is simply $\frac{\pi}{2} t_b$. Using Equation [9] the drag coefficient of the parabolic strut based on its chord may be determined as $\frac{\pi}{8} t_b^2$. The drag coefficient of this strut based on the base area C_{D_b} is therefore $\frac{\pi}{8} t_b$.

The pressure distribution and drag coefficient for base vented parabolic struts as given in the preceeding paragraph are determined from linearized theory. A more accurate non-linear result is presented in Reference 10 where the pressure distribution is given as

$$C_p = \frac{\tau^2(1-x)}{4x+\tau^2} \text{ where } \tau = \frac{t_b}{2} \qquad [10]$$

and the drag coefficient as

$$C_D = \frac{\tau^3}{2}\left[\frac{4+\tau^2}{2\tau}\left(\tan^{-1}\frac{2}{\tau}\right)-1\right] \qquad [11]$$

The value of the pressure coefficient along the chord of a parabolic base vented strut as given by Equation [10] is

plotted in Figure 3 for several values of t_b. It may be noted in Figure 3 that the linearized result (uniformly zero pressure over the chord) is a good approximation to the more exact result for values of t_b less than about .2 which includes most of the parent strut thicknesses of practical value.

The value of the drag coefficient of base vented parabolic struts as given by Equation [11] (but converted to C_{D_b}) is shown in Figure 4. The linearized result for the drag coefficient ($C_{D_b} = \frac{\pi}{8} t_b$) is also shown in Figure 4 and it may be noted that the linearized result is an excellent approximation of the more exact non-linear result even for values of t_b up to about .25.

Plate Generated Struts

The parametric equation for the cavity shape behind a two dimensional flat plate operating at zero cavitation number in an infinite fluid as given by Kirchoff (Reference 11) is:

$$\frac{x}{h} = \frac{1}{4\pi}\left[\frac{\sin\theta}{\cos^2\theta} - \ell n\, \frac{1}{\tan(\frac{\pi}{4} - \frac{\theta}{2})}\right] \qquad [12a]$$

$$\frac{y}{h} = \frac{2}{\pi+4}\left[\frac{1}{\cos\theta} + \frac{\pi}{4}\right] \qquad [12b]$$

where the origin is at the plate midpoint, h is the height of the plate, and θ is a parameter equal to the polar angle measured clockwise such that $\theta = \frac{\pi}{2}$ is the x axis. (See Figure 5). By filling in the space bounded by the plate, the cavity streamlines, and the line x = c, plate generated struts may be formed. These plate generated struts, as pointed out previously, are struts which, among all base vented ($\sigma = 0$) struts with non-negative pressures over their chord, have the least drag for a given thickness ratio.

The drag coefficient based on the frontal area of the flat plate is given by the well known equation $C_{D_{plate}} = \frac{2\pi}{4+\pi}$. Thus the drag coefficient of the plate generated strut based on the base area of the strut is given by the equation

$$C_D = \frac{2\pi}{4+\pi} \cdot \frac{2y(c)}{h} = \frac{\pi/2}{1/\cos(\theta) + \pi/4} \qquad [13]$$

The ordinates of plate generated struts having thickness-chord ratios varying between .04 and .34 have been calculated and are tabulated in Table I. Included in Table I is the value of the trailing edge slope and C_D for each thickness-chord ratio tabulated. By examining the behavior of Equations [12] and [13] for $\theta \rightarrow \frac{\pi}{2}$, the following linearized result for the drag coefficient of a plate generated strut (based on the base area) in terms of the base thickness-chord ratio may be obtained as

$$C_{D_b} = \frac{\pi + 4}{32} \frac{t_b}{c} \qquad [14]$$

It is important to note from this result that for the same thickness chord ratio the plate generated strut drag coefficient is about half that of a parabola. The linearized result given by Equation [14] is compared in Figure 6 with the exact solution obtained by carrying out the computations indicated by Equations [12] and [13] (and tabulated for discrete values of t_b/c in Table I). It may be seen that the linearized result is in excellent agreement with the exact solution for values of t_b/c less than .25.

Since the drag of a plate generated strut is significantly less than the drag of a comparable parabolic strut, it is

important to examine the differences in the shape of the two struts. In Figure 7 the non-dimensional coordinates of a plate generated strut and a parabolic strut of equal thickness-chord ratio (.2) are compared. Figure 7 shows that there is very little difference in the shape of the two struts, the most significant difference being in the flat leading edge of the plate generated strut. Thus, for purposes of determining the section modulus of plate generated struts, it is sufficient to approximate the strut by a parabolic strut of equal thickness chord-ratio. The true section modulus of the plate generated form will be slightly higher than the result obtained by using the parabolic approximation and so may be considered as conservative.

Although the plate generated strut does have minimum drag among all base vented struts with non-negative pressure coefficients along its chord, it is not the least drag strut if negative pressures are permitted over the chord. In fact, as pointed out previously, if negative pressures are permitted, base vented struts having zero drag are possible. The remainder of this report is concerned with determining the properties of such struts by adding various perturbations to either the parabolic or plate generated forms just discussed. In view of its least drag, it would seem necessary to use only the plate generated shape as a parent form. However, because of the absence of experimental data on the plate generated form and the possibility that the blunt nose of this form may lead to extreme yaw sensitivity in cavitation or ventilation inception, struts derived from the more conventional nosed parabola are also included. The parabola was also included because the strut shapes derived from the parabola may be conveniently

non-dimensionalized with respect to σ_1, and t/c; whereas such a convenient presentation was not possible with the plate generated shapes.

SPECIFIC LOW DRAG STRUT SHAPES

As pointed out in the section on parabolic struts, a parabolic strut of base thickness t_p is generated in the physical plane by a vortex of strength $\frac{\pi}{2} U_\infty t_p$ located at the origin of the airfoil plane. Such a vortex is illustrated in Figure 8. Now, if in the airfoil plane a symmetrical vorticity distribution over the interval $-1 \leq x \leq 1$ is added to the parabola producing single vortex, a modified parabolic strut will be produced in the physical plane. This modified parabola will retain the nose shape of the parent parabola but its afterbody thickness will be thinner or thicker and the pressures along the chord less than or greater than the parent parabola depending on the sign of the vorticity added in the airfoil plane.

Equation [9] shows that the drag of the modified strut varies with the square of the lift coefficient of the equivalent airfoil. Thus, if a given parent parabolic shape is modified by adding a distribution of negative vorticity in the airfoil plane, the original parabolic drag will be diminished because the total lift coefficient of the equivalent airfoil is reduced. Furthermore, if the total negative vorticity is exactly equal to the single parabola producing vortex, the lift on the equivalent airfoil will be zero and thus a zero drag strut will be produced. Obviously an infinite number of such zero drag struts are possible, each shape depending on the vorticity distribution selected.

An important design problem is to select the best of these zero drag struts.

Another important design problem might be to select a minimum drag strut whose trailing edge slope has some prescribed value. For example, struts with zero trailing edge slope seem particularly attractive. It is particularly easy to see how struts with zero trailing edge slope may be achieved by examining the induced velocity at the trailing edge of the equivalent airfoil. The distributed vorticity must be selected so as to cancel exactly the velocity due to the single parabola producing vortex. Another design problem may be to select a minimum drag strut of a given thickness at a specified location along the chord. All of these problems require the systematic investigation of a variety of vorticity distributions used to perturb the parent parabolic shape. The vorticity distributions selected for investigation and application to the problems outlined above are described in the following section.

PERTURBATION VORTICITY DISTRIBUTIONS

Fourier Series

If the perturbation vorticity distribution is described by an even series with a sufficient number of terms, essentially all distributions of significance to the strut problem may be investigated. Since a Fourier series has been particularly useful in the analagous lifting surface problem (See References 3, 5, and 6), a Fourier series perturbation distribution was applied to the strut problem and investigated.

In the equivalent airfoil plane, the horizontal perturbation velocity, $\bar{u}$, was taken to be as follows

$$\bar{u} = \sum_{n=1}^{\infty} A_n \sin(n\theta), \qquad (n, \text{ odd}) \qquad [15]$$

where θ is defined by the usual thin airfoil transformation applied to the equivalent airfoil of chord = 2 such that

$$\frac{1+\xi}{2} = \tfrac{1}{2}(1-\cos\theta) \text{ or } \xi = -\cos\theta \qquad [16]$$

Thus θ varies between 0 and π as ξ varies over the chord of the equivalent airfoil from leading edge to trailing edge. Using Equation [9] the drag coefficient due to the perturbation velocity given in Equation [15] may be determined as

$$C_D = \frac{2}{\pi}\left[\int_0^{\pi} \sum_{n=1}^{\infty} A_n \sin n\theta \cdot \sin\theta d\theta\right]^2 = \frac{\pi}{2}A_1^2 \qquad [17]$$

As pointed out in Reference 6 (and as may be deduced from Equation [8]) the drag coefficients of separate components may be added in the linearized theory to obtain total drag by taking the square of the sum of the square roots of the individual components. Thus

$$C_{D_{total}} = [\sqrt{C_{D_1}} + \sqrt{C_{D_2}}]^2 \qquad [18]$$

Now if a strut is generated by the addition of ordinates produced by the perturbation distribution of Equation [15] to the ordinates of a parent parabola, the drag coefficient of this strut will be

$$C_D = \left[\sqrt{\frac{\pi}{8}}\, t_p + \sqrt{\frac{\pi}{2}}\, A_1\right]^2 \qquad [19]$$

Equation [19] clearly reveals that a drag reduction will be achieved if the sign of A_1 is taken as negative. In fact a zero drag strut will result when $A_1 = -\frac{t_p}{2}$.

It should be noted that as long as the bracketed term in Equation [19] is positive, the total circulation on the equivalent airfoil will be positive, and the shape of the cavity far downstream will be approximately the same as if it had been generated by a single leading edge vortex. Thus the asymptotic shape of the cavity will be approximated by a simple parabolic strut whose thickness corresponds to the strength of the single vortex. On the other hand if the bracketed term in Equation [19] is negative, the total circulation on the equivalent airfoil will be negative. This net negative vorticity implies that the generated streamlines are imaginary since everywhere downstream from some point the streamlines are on opposite sides of the x axis than specified in the derivation. Consequently, in order to derive physically meaningful struts, the bracketed term in Equation [19] must be confined to non-negative values.

The value of $\frac{dy}{dx}$ due to the perturbation distribution given by Equation [15] may be determined directly from thin airfoil theory as $\sum_{n=1}^{\infty} A_n \cos(n\theta)$. Using this result and Equation [5] the perturbation ordinates may be determined as

$$y(x) = -\int_0^{\theta} \sum_{n=1}^{\infty} A_n \cos(n\theta) \sin 2\theta \, d\theta, \quad (\theta = \cos^{-1}\sqrt{x}) \qquad [20]$$

<u>One Term Modified Parabolic Struts</u>: If only the first term in Equation [15] is used, so that $\bar{u} = A_1 \sin\theta$, Equation [20] becomes

$$y_o(x) = -\int_0^{\theta} A_1 \cos\theta \sin 2\theta d\theta = \frac{2}{3} A_1 \cos^3\theta \Big]_0^{\cos^{-1}\sqrt{x}} = \frac{2}{3} A_1 x^{\frac{3}{2}} \qquad [21]$$

If the ordinates given by Equation [21] are added to those of a parent parabola the resulting strut shape will be given by the simple equation

$$y = \frac{t_p}{2} x^{\frac{1}{2}} + \frac{2}{3} A_1 x^{\frac{3}{2}} \qquad [22]$$

For this "one term" strut, if A_1 is negative the minimum pressure coefficient occurs at the leading edge (actually just aft of the leading edge) and is equal in value to $2A_1$. If this minimum pressure is set equal to the negative of the incipient vapor cavitation index $\frac{p_\infty - p_v}{\frac{1}{2}\rho U_\infty^2}$, A_1 may be replaced by $-\frac{\sigma_i}{2}$. The perturbation velocity distribution in the airfoil plane may then be written as $\bar{u} = \frac{\sigma_i}{2} \sin\vartheta = \frac{\sigma_i}{2} \sqrt{1-\xi^2}$. Since $C_p(x) = -2\bar{u}(\sqrt{x})$, the pressure coefficient on the strut in the physical plane is given by the following equation

$$\frac{C_p}{\sigma_i} = -\sqrt{1-x} \qquad [23]$$

The pressure distribution as given by Equation [23] is shown in Figure 9. The actual pressure distribution on a "one term" modified parabolic strut is obtained by adding the contributions of the perturbation and the parent parabola; that is, adding the values given by Equations [23] and [10].

A particular "one term" modified parabolic strut may be determined by specifying one additional parameter such as,

the drag coefficient, thickness at a specified location, the slope at specified location,etc. For example the shape of the zero drag, one term modified parabolic strut (for which $A_1 = \frac{t_p}{2}$ and thus $t_p = \sigma_1$) is given by the equation

$$\frac{y}{\sigma_1} = \tfrac{1}{2}x^{\frac{1}{2}} - \frac{1}{3}x^{\frac{3}{2}} \qquad [24]$$

The strut shape given by Equation [23] is shown in Figure 10.

Similarly the shape of a one term modified parabolic strut whose trailing edge slope is zero ($t_p=2\sigma_1$) is given by the equation

$$\frac{y}{\sigma_1} = x^{\frac{1}{2}} - \frac{1}{3}x^{\frac{3}{2}} \qquad [25]$$

The strut shape given by equation [24] is also shown in Figure 10 for comparison with the zero drag strut.

The drag coefficient of the strut corresponding to Equation [25] may be determined from Equation [19] as $\frac{3\pi}{32}\sigma_1$ or in terms of the base thickness of the strut, $t_b=2y(1)=\frac{4}{3}\sigma_1$, C_D becomes $\frac{9\pi}{128}t_b$. Since a parabola of equal base thickness has a drag coefficient of $\frac{\pi}{8}t_b$, it may be seen that the drag of this modified parabolic strut is about 56 per cent of the drag of a parabola of equal base thickness.

It is also important to determine the section modulus (bending about the x axis) of the struts derived. The non-dimensional section modulus $\overline{Z}$ is defined as Z/c^3 or in the present notation where c is unity $\overline{Z}$ is simply Z and may be obtained for symmetrical struts from the equation

$$\bar{Z} = \frac{\frac{2}{3}\int_0^1 y^3 dx}{y_{max}} \qquad [26]$$

Using Equation [25] the non-dimensional section modulus, $\bar{Z}$, may be computed to be .02503 σ_i^2 and .18169 $\hat{\sigma}_i^2$ for the zero drag and zero trailing edge slope struts.

Another family of one term struts may be derived by specifying the value of C_D in Equation [19]. Such a one term family has been computed for various values of $\frac{C_D}{\sigma_i^2}$ and these results are presented in Figure 11. Included in Figure 11 are computed values of the parameter $\bar{Z}/\sigma_i^2$ for each of these struts. The designer may use Figure 11 to select the "one term" strut with least drag which satisfies prescribed design values of σ_i, $\bar{Z}$, and thickness at a prescribed chordwise station.

<u>One Term Modified Plate Generated Struts:</u> Since the linearized drag coefficient of the plate generated form based on the chord is only $\frac{\pi+4}{32} t_p^2$ compared with $\frac{\pi}{8} t_p^2$ for the parabola, struts which are superior to the modified parabolic forms just described may be obtained by applying the same perturbations (as given by Equation [21]) to a plate generated parent form. Simple general expressions for the shape of such modified plate generated struts are not possible because of the dependence of the plate generated shape on the value of t_p (for a unit chord). However, the following results may be presented in terms of ordinates of the plate generated form y_p which may be calculated from Equation [12] or obtained from Table I. Thus for a one term modified plate generated strut,

$$y = y_p - 1/3\ \sigma_1 x^{\frac{3}{2}} \qquad [27]$$

where $y_p = f(t_p)$ as given by Equation [12].

The drag coefficient of this one term modified plate generated strut is given by the following equation

$$C_D = \left[\sqrt{\frac{\pi+4}{32}}\ t_p - \sqrt{\frac{\pi}{2}}\ \frac{\sigma_1}{2}\right]^2 \qquad [28]$$

so that for a zero drag strut

$$t_p = 2\sqrt{\frac{\pi}{\pi+4}}\ \sigma_1$$

and for a zero trailing edge trailing edge slope strut

$$\frac{dy_p}{dx}(t_p,1) = \tfrac{1}{2}\sigma_1 \qquad [29]$$

so that t_p becomes specified in terms of σ_1 and the drag coefficient and the shape of the struts may be evaluated for specified values of σ_1. It is emphasized here that the ordinates of these struts cannot be non-dimensionalized with respect to σ_1 as was done for the modified parabolic forms. The relationships just discussed were used to calculate the characteristics of one term modified plate generated struts (one having zero drag and one having zero trailing edge slope) for a specific value of $\sigma_1 = .1$. The shapes of these struts are shown in Figure 12 and compared with one term modified parabolic struts designed for the same value of $\sigma_1 = .1$. The value of the drag coefficient for each of these struts is also given in Figure 12. It may be noted that the modified plate generated forms are very much superior to the modified parabolic forms. That is, the thickness of the plate generated zero drag strut

is greater than that of a similar parabolic generated form and although the shapes of the zero trailing edge slope struts are very nearly the same, drag of the plate generated one is only 26 per cent of the parabolic generated strut.

It is true that the shape of the plate generated strut cannot be non-dimensionalized with respect to its base thickness; however, for thickness chord ratios less than about .2, the plate generated form can be adequately approximated by a parabola in its trailing edge region. This fact is illustrated in Figure 7 where a parabola and plate generated strut of equal base thickness ($t_p = .2$) are compared. Thus for purposes of calculating $\bar{Z}$ and trailing edge slope, the plate generated shape may be approximated by a parabola. If this approximation is made, the characteristics of modified plate generated struts may be non-dimensionalized in the same way as was done for modified parabolic forms. This approximation was made and the non-dimensional characteristics of the "one term" struts may be summarized in the following table

CHARACTERISTICS OF ONE TERM STRUTS

Parent Form	Type	σ_i/t_b	t_{max}/t_b	C_D/t_b^2	$\bar{Z}/\sigma_i^2$
Parabola	Zero Drag	3.00	1.4141	0	.025025
	Zero T. E. Slope	.750	1.00	.22089	.18169
Plate Generated	Zero Drag	1.5156	1.109	0	.110
	Zero T. E. Slope	.750	1.00	.056943	.182

The Fourier series perturbation distribution was selected with the expectation that particularly interesting low drag shapes could be obtained by taking only a few terms in the series (for example, the one term struts described above) and optimizing these coefficients so as to give maximum $\bar{\bar{Z}}$ for a given value of σ_1 and $\bar{C}_D$. This procedure would be analagous to the well known two, three and five term supercavitating hydrofoil sections. However, the addition of a second term, that is $A_n = 0(n > 3)$, resulted in a strut which was considerably inferior to the one term strut for all values of $\frac{A_3}{A_1}$. The addition of a third term, so complicated the analysis, without obvious improvement over the one term design, that the Fourier series representation of the pressure distribution was discarded in favor of so called "roof top" distributions which are often utilized in airfoil theory.

"Roof Top" Pressure Distributions: In Reference 9, the hydrodynamic comparison theorem is utilized to prove that the plate generated strut is the least drag strut (with non-negative pressures over the chord) among all struts having equal sectional area. A similar analysis may be carried out to prove that among all base vented struts having a prescribed minimum pressure coefficient or σ_1, the least drag strut for a given sectional area is a modified plate generated strut having a uniform chordwise pressure distribution such that $C_p = -\sigma_1$.

Although a constant pressure perturbation applied to the plate generated form will result in the lowest possible strut drag for a given thickness and vapor cavitation number, such a strut is subject to the criticism that the infinite

pressure gradient at the trailing edge may cause boundary layer separation and subsequent ventilation over the rearward portion of the strut. In order to design struts with less severe pressure gradients over the rearward portion, a one parameter family of distributions known as "roof top" distributions were studied. This perturbation distribution was applied in the airfoil plane and consisted of constant vorticity over the central portion of the equivalent airfoil up to an arbitrary point $\xi = \pm \sqrt{\bar{a}}$, followed by a linear reduction to zero at the leading and trailing edges of the equivalent airfoil. The pressure distributions in the physical plane which result from this "roof top" perturbation are shown in Figure 13. It may be seen that the strut chordwise pressure distribution is characterized by a constant pressure over the region $0 \leq x \leq a$, followed by a parabolic decay to zero at the trailing edge.

The characteristics of these "roof top" struts may be obtained in terms of the specified vapor cavitation number σ_i, the parameter a, and some other specification such as drag coefficient, trailing edge thickness, trailing edge slope, etc. The magnitude of the drag coefficient in terms of the strut chord and the perturbation slopes and ordinates resulting from prescribed values of σ_i and "a" are derived in the following analysis.

In the airfoil plane the "roof top" horizontal perturbation velocity distribution may be given by the following equations:

$$\bar{u}_1(\xi) = -\frac{\sigma_i}{2}\left[\frac{1+\xi}{1-\bar{a}}\right] \quad -1 \leq \xi \leq -\bar{a} \qquad [30a]$$

$$\bar{u}_2(\xi) = -\frac{\sigma_i}{2} \qquad -\bar{a} \leq \xi \leq \bar{a} \qquad [30b]$$

$$\bar{u}_3(\xi) = -\frac{\sigma_i}{2}\left[\frac{1-\xi}{1-\bar{a}}\right] \quad \bar{a} \leq \xi \leq 1 \qquad [30c]$$

where $\bar{a}$ is the location of the discontinuity in $\bar{u}$ and is numerically equal to $\sqrt{a}$.

The slope distribution of the equivalent airfoil with the $\bar{u}$ distribution given by Equation [30] may be determined from Equation [3] as

$$\frac{dy}{dx}(\xi)=\frac{1}{\pi}\left[\int_{-1}^{-\bar{a}}\frac{\bar{u}_1(\xi')d\xi'}{(\xi'-\xi)}+\int_{-\bar{a}}^{+\bar{a}}\frac{\bar{u}_2(\xi')d\xi'}{(\xi'-\xi)}+\int_{\bar{a}}^{1}\frac{\bar{u}_3(\xi')d\xi'}{(\xi'-\xi)}\right] \qquad [31]$$

After carrying out the indicated integration Equation [31] becomes

$$\frac{dy}{dx}(\xi)=-\frac{\sigma_i}{2\pi(1-\bar{a})}\left[\ell n\left|\frac{(\xi+\bar{a})(\xi-1)}{(\xi+1)(\xi-\bar{a})}\right|+\xi\,\ell n\left|\frac{\xi^2-\bar{a}^2}{\xi^2-1}\right|\right]-\frac{\sigma_i}{2\pi}\,\ell n\left|\frac{\bar{a}-\xi}{-\bar{a}-\xi}\right| \qquad [32]$$

The strut perturbation ordinates corresponding to the equivalent airfoil slopes given by Equation [32] may be determined directly from Equation [5]. The general expression for the strut perturbation ordinates may then be written as

$$\frac{y_a}{\sigma_i}=\frac{1}{6\pi(1-\sqrt{a})}\left[\begin{array}{l}2\sqrt{x}(a-1)+(3x-2x^{\frac{3}{2}}-1)\,\ell n(1-\sqrt{x})\\ -(3x+2x^{\frac{3}{2}}-1)\,\ell n(1+\sqrt{x})+(3x\sqrt{a}+2x^{\frac{3}{2}}-a^{\frac{3}{2}})\,\ell n(\sqrt{a}+\sqrt{x})\\ -+(2x^{\frac{3}{2}}-3x\sqrt{a}+a^{\frac{3}{2}})\,\ell n\,|\sqrt{a}-\sqrt{x}|\end{array}\right] \qquad [33]$$

The perturbation ordinates given by Equation [33] are tabulated for various values of a in Table II. Equation [33] is valid for $0 \leq x \leq 1$ and $0 \leq a < 1$. For the special case of $a = 1$ the perturbation ordinates may be evaluated to be

$$\frac{y_{a=1}}{\sigma_i}=\frac{1}{\pi}\left[\sqrt{x}+\frac{x-1}{2}\,\ell n\frac{1+\sqrt{x}}{1-\sqrt{x}}\right] \qquad [34]$$

The lift coefficient of the equivalent airfoil may be determined from the area under the trapezoidal pressure dist-

ribution as

$$\bar{C}_L = -\sigma_i(1+\bar{a}) \qquad [35]$$

so that the drag coefficient may be determined from Equation [9] to be

$$\sqrt{C_{D_c}} = -\frac{\sigma_i}{\sqrt{2\pi}}(1+\sqrt{\bar{a}}) \qquad [36]$$

Thus the total drag coefficient of struts obtained by "roof top" perturbations to the parent parabolic shapes will be given by the equation

$$C_{D_c} = \left[\sqrt{\frac{\pi}{8}}\, t_p - \frac{\sigma_i}{\sqrt{2\pi}}(1+\sqrt{\bar{a}})\right]^2 \qquad [37]$$

The ordinates of "roof top" struts can of course be obtained by the addition of the parent ordinates and the perturbation ordinates given by Equation [33] or [34].

<u>"Roof Top" Modified Parabolic Struts:</u> Using the parabola as a parent form, particular struts may be derived with "roof top" chordwise pressures. Of particular interest is the zero cavity drag strut. From Equation [37] it may be seen that for zero drag the value of t_p must be taken as $\frac{2\sigma_i}{\pi}(1+\sqrt{\bar{a}})$. Thus the ordinates of "roof top" modified parabolic struts which have zero cavity drag may be obtained by adding the ordinates given by Equation [33] or [34] (or Table II) to the ordinates of the parabola given by the equation

$$y/\sigma_i = \frac{1}{\pi}(1+\sqrt{\bar{a}})\sqrt{x} \qquad [38]$$

The shapes of such "roof top" modified parabolic struts with zero cavity drag are shown in Figure 14 for various values of the parameter a. Also given in Figure 14 is the calculated value of $\bar{Z}/\sigma_i^2$ for each of these struts. Comparison of the "one term" modified parabolic zero drag strut shown in Figure 9 with

the "roof top" struts shown in Figure 14 reveals that the "one term" strut is roughly similar to an a = .4 "roof top" strut. Thus it is clear from Figure 14 that "roof top" zero drag struts with a $\geq$ .4 can be made thicker than "one term" struts for a given value of σ_i.

Another family of struts may be formed by prescribing the drag coefficient to be a particular value. For modified parabolic struts of this type the strut shape becomes determined by adding the "roof top" perturbation ordinates given by Equation [33] or [34] (or Table II) to the parabola $y/\sigma_i = \frac{t_p}{2\sigma_i}\sqrt{x}$, where t_p is defined by Equation [37] for a given value of $\sqrt{C_{D/\sigma_i}}$ and a. The shape of "roof top" struts for various values of $\sqrt{C_{D/\sigma_i}}$ for the particular value of a = .9 is presented in Figure 15.

For the particular case of a zero trailing edge slope, "roof top" strut there is a unique value of the parameter $\sqrt{C_{D/\sigma_i}}$ for each value of a. This value may be determined as follows.

The trailing edge slope of a modified parabolic "roof top" strut may be evaluated by adding the perturbation component given by Equation [32] for $\xi = 1$ to the parabolic component $\frac{t_p}{4}$. Thus the trailing edge slope, m, may be determined as

$$m = \left(\frac{dy}{dx}\right)_{TE} = \pm\left[\frac{t_p}{4} - \frac{\sigma_i}{2\pi}\left(\frac{2}{1-\sqrt{a}}\ln\frac{2}{1+\sqrt{a}} + \ln\frac{1+\sqrt{a}}{1-\sqrt{a}}\right)\right] \qquad [39]$$

For the particular case of zero trailing edge slope the following relationship must be satisfied

$$\frac{t_p}{\sigma_i} = \frac{2}{\pi}\left(\frac{2}{1-\sqrt{a}}\ln\frac{2}{1+\sqrt{a}} + \ln\frac{1+\sqrt{a}}{1-\sqrt{a}}\right) \qquad [40]$$

Substitution of Equation [40] into Equation [37] results in the following equation for the drag of the zero trailing edge slope, "roof top" modified parabolic strut

$$\left(\frac{C_{D_c}}{\sigma_i}\right)_{m=0} = \frac{1}{\sqrt{2\pi}}\left[\frac{2}{1-\sqrt{a}}\ln\frac{2}{1+\sqrt{a}} + \ln\frac{1+\sqrt{a}}{1-\sqrt{a}} - (1+\sqrt{a})\right] \qquad [41]$$

The ordinates of this strut are obtained by the addition of the perturbation ordinates given by Equation [33] or [34] (or Table II) to the parent parabolic shape defined by

$y/\sigma_i = \frac{t_p}{2\sigma_i}\sqrt{x}$, where t_p/σ_i is obtained from Equation [37].

Another family of "roof top" struts may be derived by applying the "roof top" perturbations to a parent plate generated form. These struts may be specified in exactly the same manner as was done for struts derived from a parabolic parent; that is, struts having zero drag, a specified drag, or specified thickness or slope at some chordwise station may be investigated. However, as mentioned previously, it is not possible to generalize the plate generated strut characteristics because of the non-linear dependence of its shape on the parent base thickness. Since the method of obtaining the shape of this type strut has been explained and, although the method is

tedious, it is straightforward, no further analysis will be given. The "roof top" perturbation drag coefficient, ordinates, and trailing edge slope are tabulated for various values of a in Table II. The drag coefficient, ordinates and trailing edge slopes of plate generated shapes of various thickness-chord ratios are tabulated in Table I. By the simple addition of these ordinates the ordinates of any "roof top" modified plate generated strut may be obtained. The cavity drag of the strut may be obtained from Equation [18].

For comparison with the "roof top" modified parabolic struts, several specific "roof top" modified plate generated struts have been derived. In Figure 16 parabolic and plate generated "roof top" struts designed for $a = .8$, $\sigma_i = .1$ for both zero cavity drag and zero trailing edge slope are presented. It may be seen that the plate generated struts are considerably thicker than the parabolic struts for the conditions specified.

SELECTION OF A BASE-VENTED STRUT DESIGN FOR OPERATION AT ZERO BASE CAVITATION NUMBER

In the preceeding analysis the characteristics of base vented struts having a variety of chordwise pressure distribution have been derived. It was shown that, in a non-viscous fluid, the minimum cavity drag strut for a given value of σ_i and a section modulus, is the plate generated strut modified with the $a = 1.0$ "roof top" pressure distribution. However, this minimum drag strut has an infinite adverse pressure gradient at its trailing edge which may cause boundary layer separation and the non-viscous fluid theory used to derive the strut will not be applicable. Furthermore, the flat nose of the minimum

drag strut may cause the chordwise vapor cavitation and ventilation inception properties of the strut to be extremely sensitive to yaw. These speculations can be answered only by experimental research which has not yet been conducted. If the yaw sensitivity problem is a real one, the struts with parabolic parent forms should improve the performance. If trailing edge separation does occur for a=1 "roof top" struts, then "roof top" struts having lesser values of "a" should improve the performance. Without this experimental background, a conservative strut design such as the "one term" modified parabola is recommended. HYDRONAUTICS, Incorporated has utilized the "one term" modified parabola with zero trailing edge slope in several hydrofoil system designs. In at least one case the strut has been investigated experimentally and found to operate satisfactorily. In these designs it was noted that the "one term" zero slope strut is very nearly equivalent to an NACA 16 series section which has been cut off at its maximum thickness. Consequently, the characteristics of such a truncated 16 series section should be equivalent to the "one term" modified parabola with zero trailing edge slope.

THE EFFECT OF FINITE CAVITATION NUMBER

All of the preceeding analysis has dealt with base vented struts operating with the base cavitation number equal to zero. Actually the base cavitation number is always finite in a real hydrofoil system because of the hydrostatic pressure gradient. Thus, if the cavity pressure is assumed to be equal to the atmospheric pressure, the base cavitation number will vary along the strut according to the following equation

$$\sigma_b = \frac{2gh}{V^2} = 2/F^2 \qquad [42]$$

where h is the vertical distance from the water surface to a point on the strut and F is the Froude Number based on this depth $\frac{V}{\sqrt{gh}}$. It is well known that the drag coefficient of a strut operating with a finite base cavitation number is greater than if the base cavitation number is zero. Thus, it is important to determine quantitatively the effect of finite base cavitation number on the drag coefficient of the struts derived.

If the base cavitation number is not zero, the strut problem illustrated in Figure 1 is modified in the following ways:

a. the base cavity length becomes a finite length, ℓ.

b. the pressure coefficient along the streamlines is not zero, but $(-\sigma_b)$.

Using linearized theory Tulin solved this finite cavitation problem in Reference 7. The important results of this analysis may be summarized as follows:

1. The cavity is approximately elliptic in shape (for small values of σ) with a cavity length to maximum width ratio given by the relationship

$$\frac{\ell}{t_{max}} = \frac{2\left(1+\frac{\sigma_b}{2}\right)}{\sigma_b} \qquad [43]$$

2. The length of the cavity formed behind arbitrary struts may be obtained from the following equation

$$\frac{\sigma_b}{\left(1+\frac{\sigma_b}{2}\right)} \frac{\pi}{4} \ell = \int_0^1 \left(\frac{dy}{dx}\right) \frac{\sqrt{\ell-(x-1)}}{\sqrt{1-x}}\, dx \qquad [44]$$

where $\frac{dy}{dx}$ is the local slope of the strut.

3. The drag coefficient of arbitrary struts is obtained from the equation

$$C_{D_c} = \frac{1}{t_b}\left[2\sigma_b\sqrt{1+\sigma_b}\int_0^1 \left(\frac{dy}{dx}\right)\frac{\sqrt{x-\ell}}{\sqrt{x-1-\ell}}dx + \frac{2\ell}{\pi}(1+\sigma_b)\left[\int_0^1 \left(\frac{dy}{dx}\right)\frac{dx}{\sqrt{(x-1)(x-1-\ell)}}\right]^2\right] \quad [45]$$

where t_b = the strut base thickness.

If the analytic expressions defining the strut shape are very complicated, the integrations indicated in Equations [44] and [45] become rather tedious. However, for the simple cases of wedge and parabolic struts where

$$\frac{dy}{dx} = \frac{t_b}{2} \text{ and } \frac{t_b}{4}x^{\frac{1}{2}}$$

respectively, the integrals may be readily evaluated. The results of such computations for the drag coefficient and cavity length for wedge and parabolic struts are presented in Figure 17 and 18. It should be noted that the drag coefficients presented in Figure 17 are based on the base area rather than the chord. Among the low drag struts developed in the preceeding sections of this report only the "one term" modified parabolic struts lead to readily integrable solutions. for the cavity length and drag coefficient. The results of such computations are also presented in Figure 17 and 18 for the "one term" zero trailing edge strut and for the "one term" zero drag strut. Again the drag coefficients presented in Figure 17 are based on the base area rather than the chord.

It is important to note in Figure 17 that for values of $\frac{\sigma_b}{t_b(2+\sigma_b)}$ greater than about 1, the drag coefficient of all of the struts except the zero drag strut become independent

of the strut shape. Figure 17 gives the first impression that at high values of $\frac{\sigma_b}{t_b(2+\sigma_b)}$, the drag of the "zero cavity drag" strut is greater than the other strut shapes. However, it should be noted that in order to house a given diameter shaft or provide a given value of section modulus it is the strut maximum thickness which is important rather than the base thickness. For the three finite ($\sigma = 0$) drag struts the base thickness and maximum thickness are identical; whereas, the zero drag ($\sigma = 0$) strut has a maximum thickness equal to $\sqrt{2}t_b$. In order to compare the drag coefficients on the basis of maximum thickness the dashed curve for the "zero drag" strut is presented in Figure 17. The coordinates for this dashed curve are based on the strut maximum thickness, that is

$$\frac{C_{D_{t_m}}}{t_m(1+\sigma_b)} \quad \text{and} \quad \frac{\sigma_b}{t_m(2+\sigma_b)} .$$

The results presented in Figures 17 and 18 were derived for specific strut shapes; however, it may be shown that the drag coefficients and cavity length

$$\frac{C_{D_b}}{(1+\sigma_b)t_b} \quad \text{and} \quad \ell$$

for struts operating at finite values of $\frac{\sigma_b}{t_b(2+\sigma_b)}$ are very nearly independent of the shape and primarily dependent on $\frac{C_{D_{b(\sigma=0)}}}{t_b}$ only. Consequently, Figures 17 and 18 may be utilized more generally by considering the curves presented as applicable

to arbitrary shaped struts with specific values of the parameter $\frac{C_{D_{b,\sigma=0}}}{t_b}$.

THE EFFECT OF FRICTIONAL RESISTANCE ON STRUT DESIGN

It is important to note that all of the preceding analysis in this report has been directed toward the determination of the cavity drag of various strut sections. The total drag of these struts operating in a real fluid will be composed of this cavity drag plus the frictional resistance of the strut. This frictional resistance component will depend on the operating Reynolds Number and may be obtained from flat plate frictional resistance data.

When the base cavitation number is small, the frictional resistance of a strut usually represents a large percentage of the total drag. For example, the total drag coefficient (based on chord), for a 10 percent thick "one term" (m = 0) modified parabolic strut operating at an average base cavitation number of .03 and a Reynolds Number based on chord of 10^8, is composed of $C_{D_{cavity}} = .005$ and $C_{D_{friction}} = .0042$. Obviously if lower cavity drag struts are investigated the frictional resistance may become the major portion of the resistance.

In some design problems, it is possible to reduce the frictional resistance contribution to the drag of a strut of prescribed $\bar{Z}$, σ_i, t, etc. by employing an annex to the basic strut as illustrated in Figure 19. The annex geometry is selected so as to remain inside the cavity produced by the forebody. In this manner, section modulus may be added to

the strut witho ' incurring additional drag.

COMPARISON OF THEORY WITH EXPERIMENT

Unfortunately, very little experimental data exists for base vented struts and that which has been obtained are for finite aspect ratio, parabolic struts only. No experimental data have been published for any of the more refined struts derived in the predeeding sections.

The experimental data which are available were obtained in the pendulum facility of Dynamic Developments Incorporated and is reported in Reference 2. These tests were performed on parabolic strut sections with base thickness-chord ratios of .1667 and .21. The struts were attached to the lower end of a falling arm pendulum with the lower end at varying depths below the water surface (measured at the bottom of the pendulum swing at which time the drag was also measured).

It is important to note that in these experiments, no foil or end plate was attached to the lower end of the strut. The base of the strut was naturally vented to the atmosphere and pressure measurements over the base of the strut revealed essentially atmospheric pressure over the entire strut base. Consequently, the base cavitation number at arbitrary depths along the strut is given by Equation [42] to be $2F^2$. The cavitation number then varies linearly along the length of the strut and if drag is taken to vary linearly with σ, the average or effective cavitation number to be used in determining the drag coefficient of the strut will be $1/F_o^2$ or $\frac{\gamma h_o/2}{\frac{1}{2}\rho U_\infty^2}$, where h_o is the depth of the bottom of the strut.

Therefore the drag coefficient data are presented as functions $1/F_o^2$ in Reference 2. These data are reproduced in Figures 20 and 21 for the 16.67 and 21 per cent thick struts respectively. Included in Figures 20 and 21 are the theoretical frictionless drag coefficients obtained from Figure 17. These theoretical coefficients, increased for both laminar and turbulent friction, are also presented in the Figures. It may be seen in Figure 20 that the agreement between theory and experiment for the 16.67 per cent thick strut is very good for values of $1/F_o^2$ greater than about .02. However, Figure 21 shows that for the 21 per cent thick strut, the theoretical values are nearly twice the values determined in the experiment.

In view of the excellent agreement between the linear and non-linear theory for the drag coefficient of parabolic struts (see Figure 4), the disagreement between theory and experiment shown in Figure 21 cannot be attributed to the invalidity of linearized theory applied to such a thick strut. The difference might be attributable to some abnormality of the pendulum experimental technique which, for example results in inherently unsteady flows. On the other hand, if the technique is indeed valid then the observed disagreement must be attributed to the three dimensional influences.

Although Figure 20 indicates that decreasing aspect ratio tends to decrease the drag coefficient of a given strut, Figure 21 fails to confirm this trend.

However, if the aspect ratio is based on the length of the strut-cavity combination rather than the strut chord, this strut-cavity aspect ratio becomes almost independent of the geometric aspect ratio at very small values of $1/F_o^2$. The

observed lack of dependence of the drag coefficient on geometric aspect ratio at low values of $1/F_o^2$ may be partially attributed to the more likely dependence of the flow characteristics on the aspect ratio based on the combined length of the strut chord and its cavity.

Some insight into the effect of finite aspect ratio on the drag of struts may be obtained by noting that at the tip of a strut of semi-infinite span, the pressures must be exactly one-half those which occur on a completely two dimensional strut. Thus the sectional drag of the tip of a strut whose span is finite (rather than semi-infinite) must be less than one half the drag of a two dimensional section. At very low aspect ratios where the span of the strut becomes about equal to the base thickness, it seems reasonable to expect that the drag coefficient of the strut (based on base area) should be about the same as the drag coefficient of a similar body of revolution.

In Reference 10 the drag coefficient of paraboloids operating at zero cavitation number is given as .00155 and .0027 for fineness ratios comparable to the 16.7 and 21 per cent thick struts. These values are indicated by the solid symbols in Figures 20 and 21. It is interesting to note that the experimental data shown in Figure 20 for low values of $1/F_o^2$ (particularly for the lowest geometric aspect ratio data) do tend toward the values predicted from the axisymmetric theory. Unfortunately data were not obtained on these struts with a hydrofoil or end plate attached to the bottom. Certainly the effect of such an end plate would be to increase the strut drag coefficients toward their theoretical two dimensional values.

In view of the inconsistencies of the data (for example, at values of $1/F_o^2$ greater than .025, the drag coefficient of the 16.67 percent strut is greater than the drag of the 21 per cent strut) and the absence of end plate data, it is difficult to draw any conclusions from the comparison of theory and experiment presented in Figures 20 and 21. However, the available data do support the speculation that the theoretical drag coefficients determined for two dimensional struts will be conservative when applied to three dimensional designs. The degree to which the two dimensional theory overestimates the drag must depend on the end conditions of the strut. If the lower end of the strut is fastened to a pod or hydrofoil, the overestimate of the cavity drag by two dimensional theory is expected to be small.

CONCLUDING REMARKS

Several families of two dimensional base vented struts have been derived which will enable the strut designer to select optimum strut sections for prescribed values of the operating vapor cavitation number, section modulus, strut slopes or maximum thickness locations. The drag coefficient of these struts operating with finite base cavitation number is also presented.

Since no experimental data are presently available for the low drag struts discussed (except for parabolic struts), the designer must complement the information presented in this report with experimental investigation. Experiment is particularly required to clarify the yaw sensitivity of base vented struts to chordwise ventilation and cavitation, and for zero yaw, to select chordwise pressure distributions which will

permit attached flow up to the trailing edge.

When derived low cavity drag struts are utilized, the total strut drag may become predominantly skin friction. Therefore, optimum strut configurations utilizing inventive devices to increase strut strength without adding drag become attractive. The trailing edge annex operating within the base cavity should therefore be considered by the designer as an important method of optimizing a given strut design.

A comparison of the two dimensional drag coefficients of parabolic struts operating at finite values of the base cavitation number with experimental data obtained on surface piercing, free-ended, struts of finite aspect ratio reveals some disagreement between theory and experiment. However, the inconsistencies in the comparison do not warrant definite conclusions other than the fact that two dimensional cavity drag coefficients will be conservative. In practical applications where the strut end is fastened to a pod or hydrofoil, the two dimensional theory should be adequate for design purposes.

REFERENCES

1. Christopher, Kenneth W. and Johnson, Virgil E., Jr., "Experimental Investigation of Aspect Ratio - 1 Supercavitating Hydrofoils at Speeds Up To 185 Feet Per Second", NASA Technical Note D-187, January 1960.

2. Andrews, Thomas M., "Foil Strut Pendulum Tests", Dynamic Developments Incorporated Report, Contract Nonr 2852(00), October 1961.

3. Tulin, Marshall P. and Burkart, M. P., "Linearized Theory for Flows About Lifting Foils at Zero Cavitation Number", DTMB Report C-638, February 1955.

4. Wu, T. Yao-Tsu, "A Free Streamline Theory for Two-Dimensional Fully Cavitated Hydrofoils", Report No. 21-17, Contract Nonr-24420, C.I.T. Hydrodynamics Laboratory, July 1955.

5. Johnson, Virgil E., Jr., "Theoretical and Experimental Investigation of Supercavitating Hydrofoils Operating Near the Free Water Surface", NASA Technical Report R-93, 1961.

6. Auslaender, Jacob, "The Linearized Theory for Supercavitating Hydrofoils Operating at High Speed Near a Free Surface", HYDRONAUTICS, Incorporated Technical Report 001-5, June 1961.

7. Tulin, Marshall P., "Steady Two-Dimensional Cavity Flows About Slender Bodies", David Taylor Model Basin Report 834, May 1953.

8. Fabula, Andrew G., "Application of Thin Airfoil Theory to Hydrofoil with Cut-Off Ventilated Trailing Edge", Naval Ordnance Test Station TP 2547, September 1960.

9. Tulin, Marshall P., "Supercavitating Foils and Struts", Paper Number 16, Symposium on Cavitation in Hydrodynamics, September 1955, National Physical Laboratory, Teddington, England.

REFERENCES (Continued)

10. Johnson, Virgil E., Jr. and Rasnick, Thomas A., "The Drag Coefficient of Parabolic Bodies of Revolution Operating at Zero Cavitation Number and Zero Angle of Yaw", National Aeronautics and Space Administration TR R-86, 1961.

11. Kirchoff, "Zur Theorie Freier Flüssegkeitsstrahlen", Crelle LXX, 1869.

TABLE - Ia.

PLATE GENERATED PARENT FORMS

x,y- PERCENT CHORD
m- TRAILING EDGE SLOPE

x/c	t_p=.04 y/c	t_p=.06 y/c	t_p=.08 y/c	t_p= .10 y/c
0	.0401	.0900	.1593	.2480
1	.2092	.3216	.4398	.5641
2	.2913	.4441	.6021	.7656
3	.3545	.5384	.7272	.9210
4	.4077	.6180	.8328	1.0524
5	.4547	.6881	.9260	1.1684
10	.6389	.9636	1.2920	1.6242
15	.7803	1.1751	1.5731	1.9745
20	.8996	1.3535	1.8103	2.2701
25	1.0046	1.5107	2.0193	2.5305
30	1.0996	1.6528	2.2082	2.7661
35	1.1870	1.7835	2.3820	2.9828
40	1.2683	1.9051	2.5438	3.1844
45	1.3446	2.0194	2.6958	3.3739
50	1.4169	2.1275	2.8395	3.5531
55	1.4856	2.2303	2.9763	3.7236
60	1.5512	2.3285	3.1069	3.8864
65	1.6142	2.4227	3.2322	4.0427
70	1.6748	2.5134	3.3528	4.1930
75	1.7332	2.6008	3.4691	4.3381
80	1.7898	2.6855	3.5816	4.4784
85	1.8446	2.7675	3.6907	4.6144
90	1.8978	2.8471	3.7966	4.7464
95	1.9495	2.9245	3.8996	4.8749
100	2.0000	3.0000	4.0000	5.0000
$\sqrt{c_{D_p}}$	.0188009	.0281450	.0374466	.0467118
m	.0099429	.0148875	.0198085	.0247123

TABLE - Ib.

PLATE GENERATED PARENT FORMS

x,y- PERCENT CHORD
m- TRAILING EDGE SLOPE

x/c	t_p=.12 y/c	t_p=.14 y/c	t_p=.16 y/c	t_p=.18 y/c
0	.3552	.4811	.6259	.7879
1	.6945	.8314	.9750	1.1249
2	.9345	1.1092	1.2899	1.4763
3	1.1200	1.3243	1.5341	1.7493
4	1.2769	1.5064	1.7411	1.9808
5	1.4154	1.6672	1.9240	2.1855
10	1.9602	2.3003	2.6445	2.9927
15	2.3792	2.7875	3.1993	3.6146
20	2.7328	3.1987	3.6677	4.1398
25	3.0445	3.5612	4.0807	4.6030
30	3.3263	3.8891	4.4543	5.0220
35	3.5856	4.1907	4.7980	5.4075
40	3.8270	4.4715	5.1180	5.7665
45	4.0537	4.7353	5.4187	6.1038
50	4.2682	4.9848	5.7031	6.4228
55	4.4722	5.2222	5.9736	6.7264
60	4.6671	5.4490	6.2322	7.0164
65	4.8541	5.6666	6.4801	7.2947
70	5.0341	5.8760	6.7188	7.5624
75	5.2077	6.0780	6.9491	7.8208
80	5.3756	6.2735	7.1718	8.0708
85	5.5384	6.4629	7.3877	8.3130
90	5.6965	6.6468	7.5974	8.5483
95	5.8502	6.8257	7.8013	8.7771
100	6.0000	7.0000	8.0000	9.0000
$\sqrt{c_{D_p}}$	.0559031	.0650657	.0742085	.0832604
m	.0295583	.0343945	.0392305	.0439894

TABLE -Ic.

PLATE GENERATED PARENT FORMS

x,y- PERCENT CHORD
m TRAILING EDGE SLOPE

x/c	t_p=.20 y/c	t_p=.22 y/c	t_p=.24 y/c	t_p=.26 y/c
0	.9681	1.1663	1.3811	1.6127
1	1.2817	1.4453	1 6155	1.7923
2	1.6688	1.8675	2.0722	2.2828
3	1.9702	2.1968	2.4289	2.6666
4	2.2260	2.4765	2.7322	2.9932
5	2.4522	2.7241	3.0008	3.2827
10	3.3452	3.7019	4.0627	4.4277
15	4.0336	4.4563	4.8825	5.3124
20	4.6151	5.0937	5.5755	6.0605
25	5.1281	5.6562	6.1871	6.7208
30	5.5923	6.1652	6.7406	7.3185
35	6.0194	6.6336	7.2500	7.8686
40	6.4171	7.0697	7.7243	8.3810
45	6.7907	7.4795	8.1701	8.8625
50	7.1442	7.8673	8.5919	9.3181
55	7.4806	8.2362	8.9932	9.7516
60	7.8019	8.5887	9.3767	10.1658
65	8.1103	8.9269	9.7446	10.5633
70	8.4070	9.2524	10.0987	10.9458
75	8.6933	9.5665	10.4404	11.3150
80	8.9703	9.8703	10.7709	11.6721
85	9.2387	10.1648	11.0913	12.0183
90	9.4994	10.4508	11.4025	12.3544
95	9.7530	10.7290	11.7051	12.6814
100	10.0000	11.0000	12.0000	13.0000
$\sqrt{c_{D_p}}$	.0922933	.1012982	.1102313	.1191183
m	.0487482	.0534972	.0581885	.0628498

TABLE -Id.

PLATE GENERATED PARENT FORMS

x,y- PERCENT CHORD
m- TRAILING EDGE SLOPE

x/c	t_p=.28 y/c	t_p=.30 y/c	t_p=.32 y/c	t_p=.34 y/c
0	1.8616	2.1265	2.4086	2.7057
1	1.9762	2.1665	2.3637	2.5675
2	2.4998	2.7227	2.9520	3.1871
3	2.9102	3.1592	3.4144	3.6750
4	3.2598	3.5316	3.8091	4.0918
5	3.5697	3.8619	4.1594	4.4619
10	4.7971	5.1707	5.5488	5.9309
15	5.7461	6.1834	6.6246	7.0694
20	6.5488	7.0404	7.5354	8.0335
25	7.2576	7.7971	8.3398	8.8852
30	7.8992	8.4823	9.0682	9.6565
35	8.4897	9.1131	9.7388	10.3669
40	9.0398	9.7006	10.3636	11.0286
45	9.5568	10.2529	10.9509	11.6506
50	10.0460	10.7754	11.5066	12.2393
55	10.5114	11.2727	12.0354	12.7995
60	10.9563	11.7479	12.5409	13.3350
65	11.3831	12.2040	13.0259	13.8489
70	11.7939	12.6428	13.4927	14.3435
75	12.1904	13.0664	13.9432	14.8208
80	12.5739	13.4762	14.3791	15.2826
85	12.9456	13.8734	14.8016	15.7303
90	13.3067	14.2592	15.2120	16.1650
95	13.6579	14.6344	15.6111	16.5879
100	14.0000	15.0000	16.0000	17.0000
$\sqrt{c_{D_P}}$	.1279787	.1367826	.1455716	.1542904
m	.0675020	.0721123	.0767258	.0812818

TABLE -IIa.

ROOF TOP PERTURBATION ORDINATES

x,y- PERCENT CHORD
m- TRAILING EDGE SLOPE

x/c	a=0 $\bar{y}/c/\sigma_i$	a=.1 $\bar{y}/c/\sigma_i$	a=.2 $\bar{y}/c/\sigma_i$	a=.3 $\bar{y}/c/\sigma_i$
0	.0000	.0000	.0000	.0000
1	.0771	.0360	.0310	.0283
2	.1973	.1027	.0882	.0805
3	.3400	.1903	.1630	.1485
4	.4988	.2957	.2523	.2296
5	.6705	.4173	.3545	.3222
10	1.6604	1.2574	1.0332	.9315
15	2.7940	2.5069	1.9665	1.7531
20	4.0183	3.9823	3.1725	2.7732
25	5.3051	5.5958	4.7235	3.9999
30	6.6360	7.3040	6.4797	5.4738
35	7.9980	9.0795	8.3660	7.2805
40	9.3809	10.9022	10.3424	9.2878
45	10.7766	12.7571	12.3819	11.4218
50	12.1784	14.6318	14.4640	13.6419
55	13.5803	16.5157	16.5723	15.9195
60	14.9767	18.3997	18.6929	18.2322
65	16.3628	20.2754	20.8136	20.5615
70	17.7336	22.1348	22.9232	22.8909
75	19.0843	23.9700	25.0107	25.2052
80	20.4096	25.7731	27.0654	27.4895
85	21.7041	27.5353	29.0758	29.7287
90	22.9609	29.2465	31.0287	31.9056
95	24.1713	30.8933	32.9071	33.9985
100	25.3193	32.4524	34.6814	35.9707
$\sqrt{c_{D_a}}/\sigma$	-.3989422	-.5250988	-.5773546	-.6174519
m/σ	.2206356	.2989937	.3394588	.3762257

TABLE - IIb.

ROOF TOP PERTURBATION ORDINATES

x,y- PERCENT CHORD
m TRAILING EDGE SLOPE

x/c	a=.4 y/c/σ_1	a=.5 y/c/σ_1	a=.6 y/c/σ_1	a=.7 y/c/σ_1
0	.0000	.0000	.0000	.0000
1	.0265	.0251	.0241	.0232
2	.0753	.0714	.0683	.0658
3	.1388	.1316	.1259	.1212
4	.2144	.2032	.1944	.1871
5	.3007	.2849	.2724	.2622
10	.8661	.8185	.7814	.7512
15	1.6222	1.5289	1.4569	1.3987
20	2.5505	2.3958	2.2782	2.1839
25	3.6473	3.4122	3.2367	3.0976
30	4.9193	4.5784	4.3301	4.1359
35	6.3855	5.9004	5.5604	5.2990
40	8.0958	7.3918	6.9337	6.5897
45	10.1473	9.0775	8.4608	8.0143
50	12.4027	11.0167	10.1598	9.5824
55	14.7833	13.3212	12.0621	11.3090
60	17.2451	15.8384	14.2384	13.2172
65	19.7557	18.4794	16.8227	15.3463
70	22.2893	21.1928	19.6333	17.7854
75	24.8229	23.9395	22.5623	20.7036
80	27.3355	26.6864	25.5444	23.8648
85	29.8061	29.4024	28.5267	27.1233
90	32.2117	32.0556	31.4598	30.3822
95	34.5245	34.6083	34.2891	33.5505
100	36.6981	37.0003	36.9325	36.5045
$\sqrt{c_{D_a}}/\sigma$	-.6512555	-.6810370	-.7079616	-.7327213
m/σ	.4131599	.4526380	.4972659	.5511652

TABLE - IIe.

ROOF TOP PERTURBATION ORDINATES

x,y- PERCENT CHORD
m TRAILING EDGE SLOPE

x/c	a=.8 $y/c/\sigma_1$	a=.9 $y/c/\sigma_1$	a=1.0 $y/c/\sigma_1$
0	.0000	.0000	.0000
1	.0224	.0218	.0212
2	.0637	.0618	.0602
3	.1173	.1139	.1109
4	.1810	.1757	.1711
5	.2536	.2461	.2396
10	.7258	.7041	.6850
15	1.3501	1.3085	1.2723
20	2.1057	2.0391	1.9812
25	2.9829	2.8857	2.8017
30	3.9772	3.8436	3.7285
35	5.0875	4.9107	4.7593
40	6.3152	6.0875	5.8937
45	7.6638	7.3762	7.1330
50	9.1397	8.7810	8.4804
55	10.7520	10.3084	9.9404
60	12.5142	11.9675	11.5199
65	14.4458	13.7710	13.2281
70	16.5771	15.7369	15.0776
75	18.9599	17.8920	17.0864
80	21.7157	20.2781	19.2800
85	25.0789	22.9714	21.6982
90	28.6896	26.1687	24.4092
95	32.3013	30.2545	27.5581
100	35.6817	34.3445	31.8309
$\sqrt{c_D}_a/\sigma$	-.7557670	-.7774121	-.7978845
m/σ	.6230326	.7400609	∞

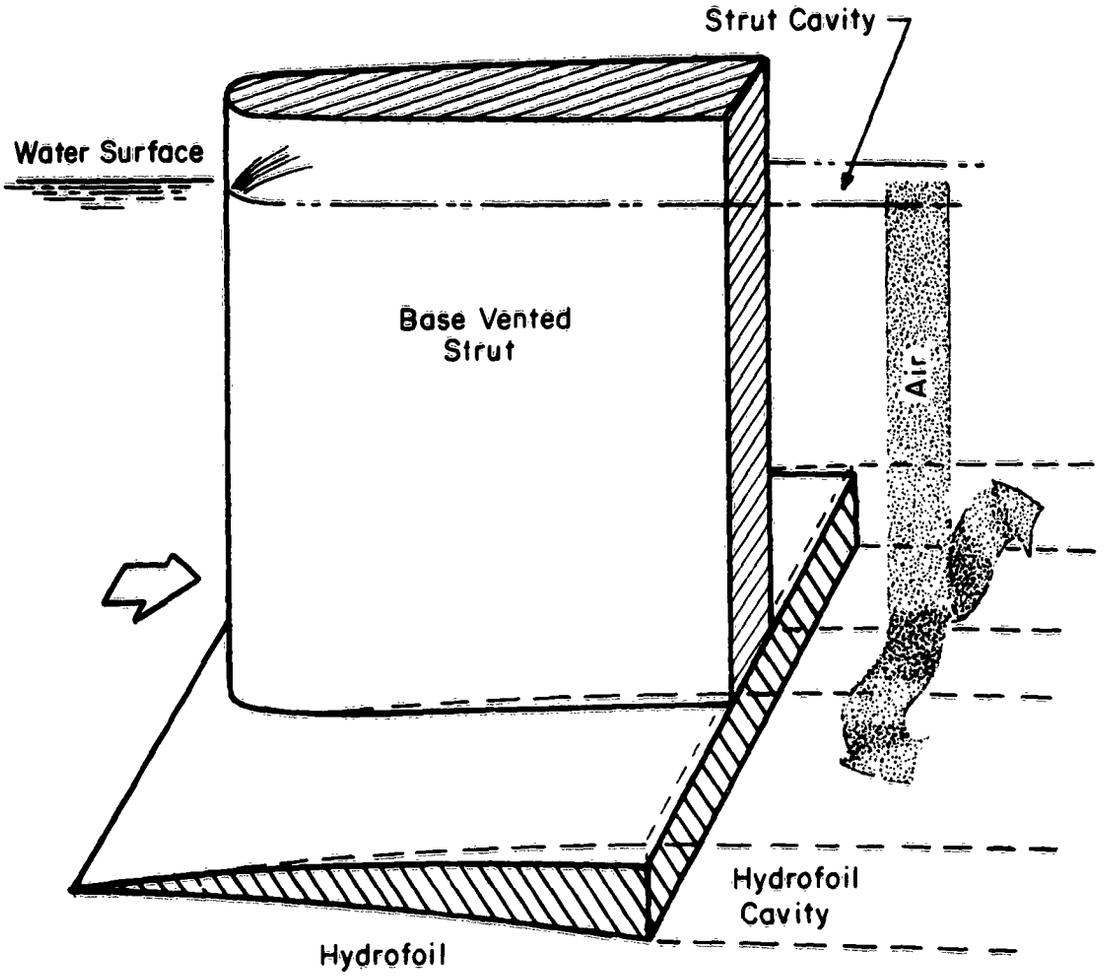

Figure 1- Base Vented Strut - Supercavitating Hydrofoil Configuration

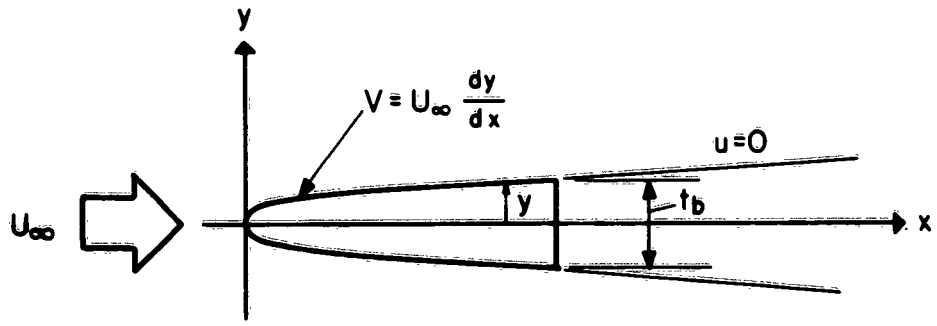

2a - Physical Plane

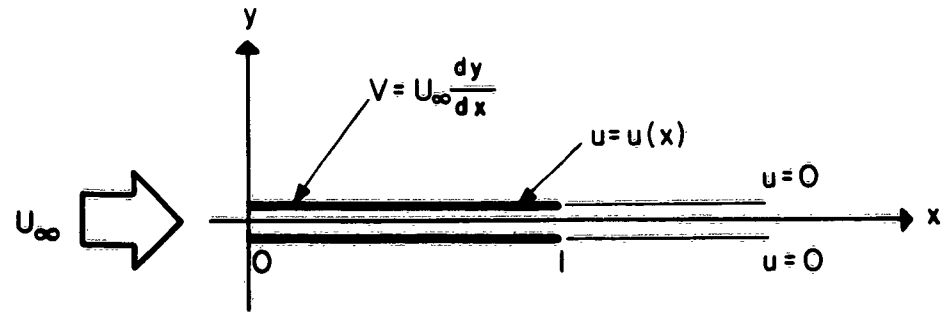

2b - Linearized Physical Plane

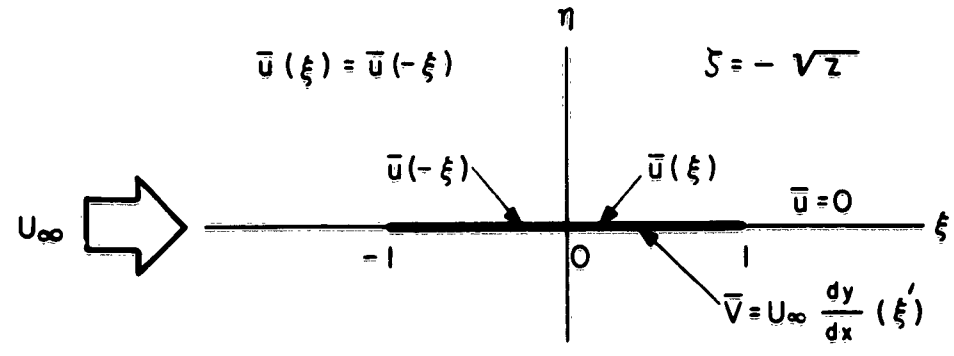

2c - Equivalent Airfoil, ζ, Plane

Figure 2 - Linearization of Base Vented Strut Problem

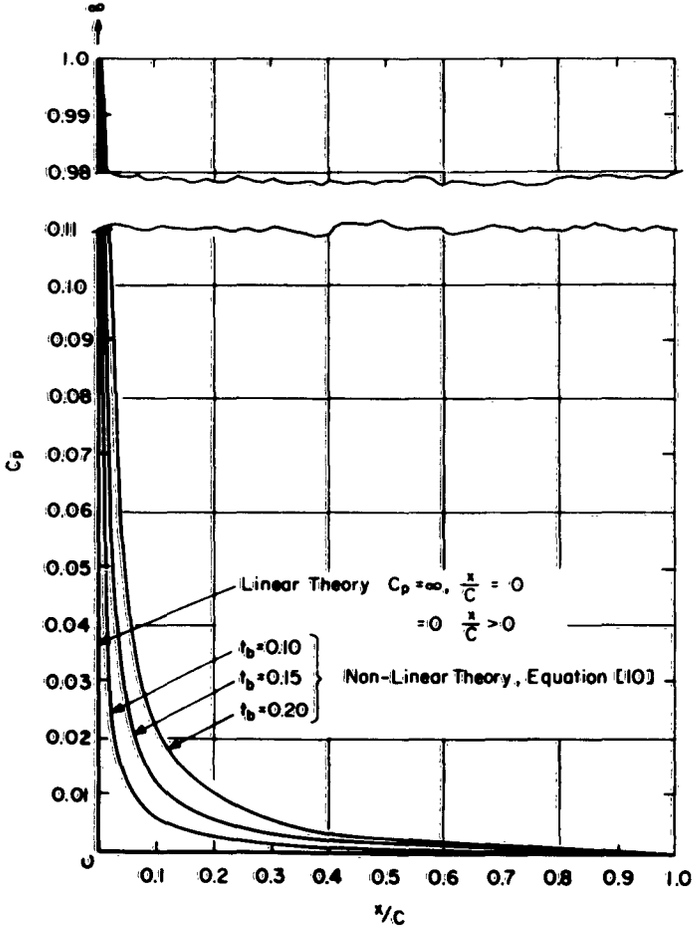

Figure 3 - Chordwise Pressure Distribution on Parabolic Struts

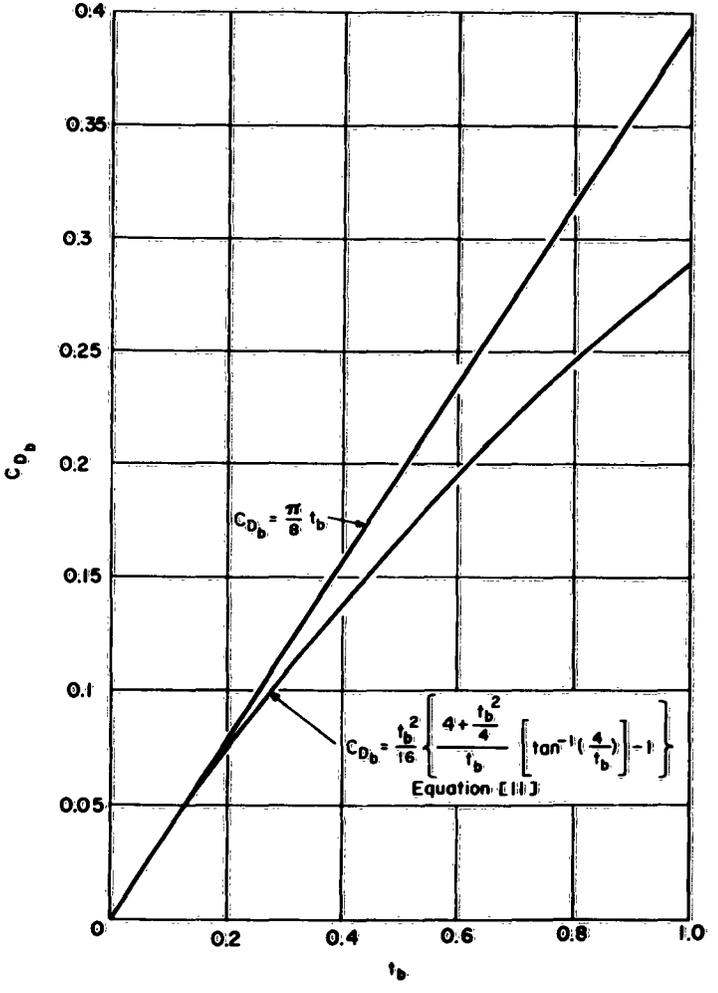

Figure 4 - Drag Coefficient of Parabolic Struts ($\sigma_b = 0$)

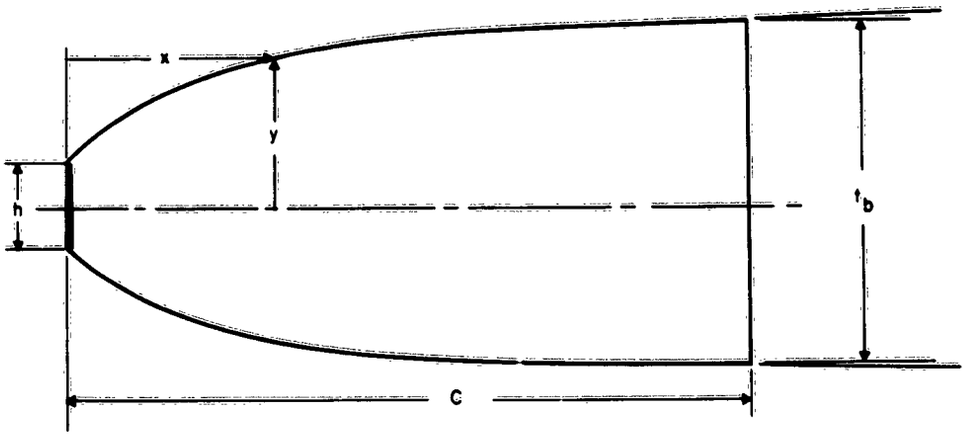

Figure 5- Definition Sketch for the Plate Generated Form

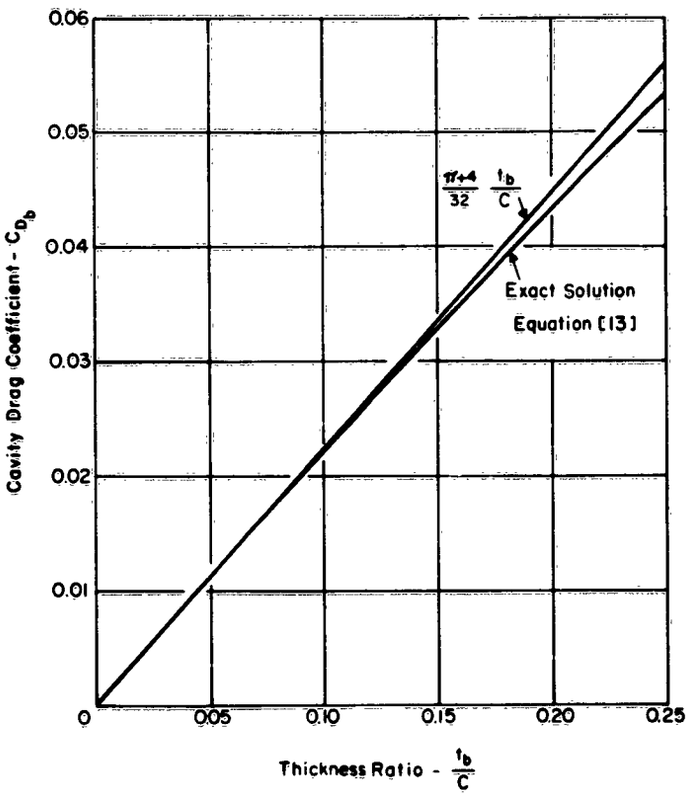

Figure 6- Exact and Approximate Solution of Cavity Drag Coefficient versus Thickness Ratio for the Plate Generated Form

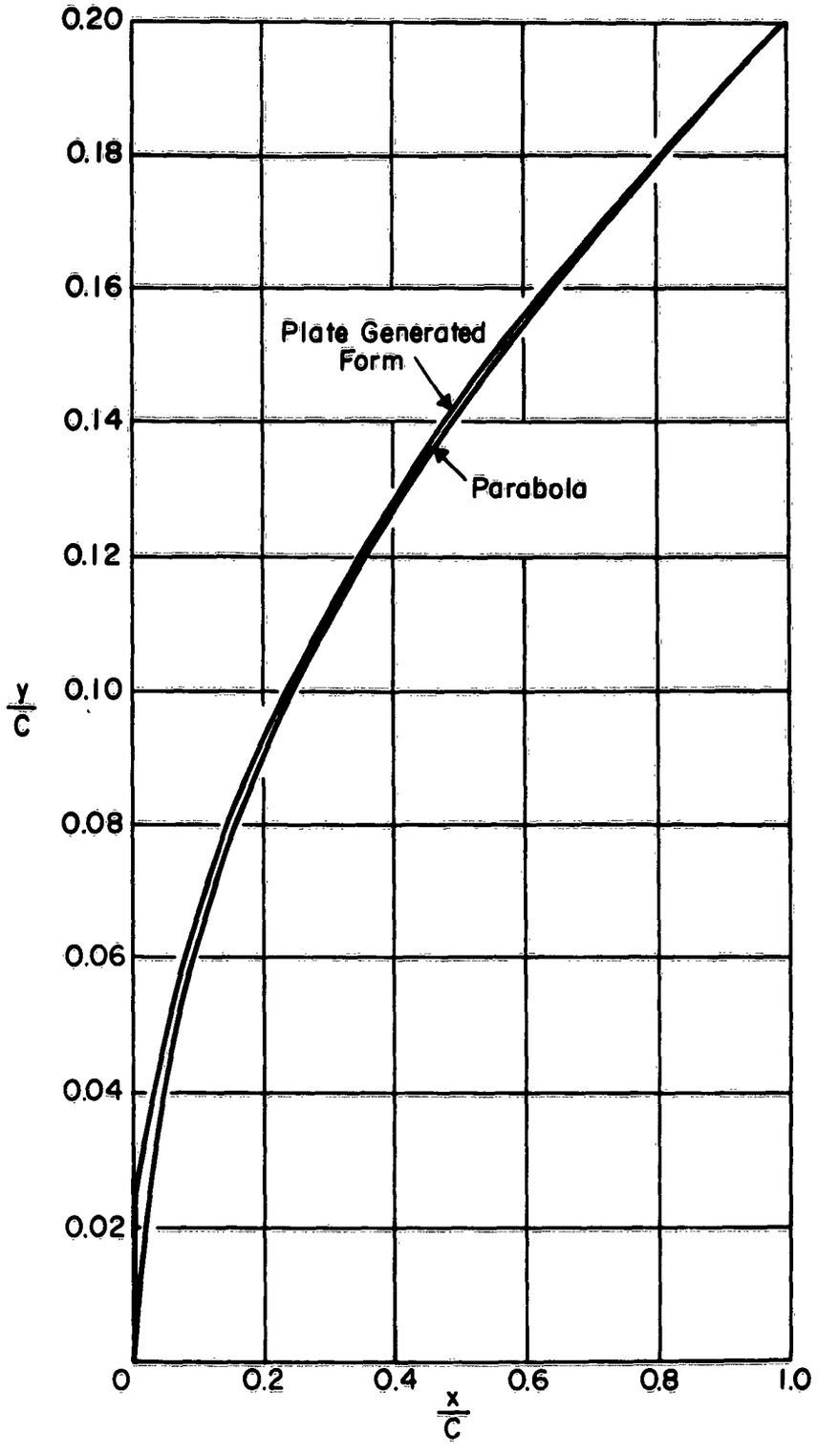

Figure 7- Shape Comparison of Plate Generated Form and Parabola $t_b = 0.20$

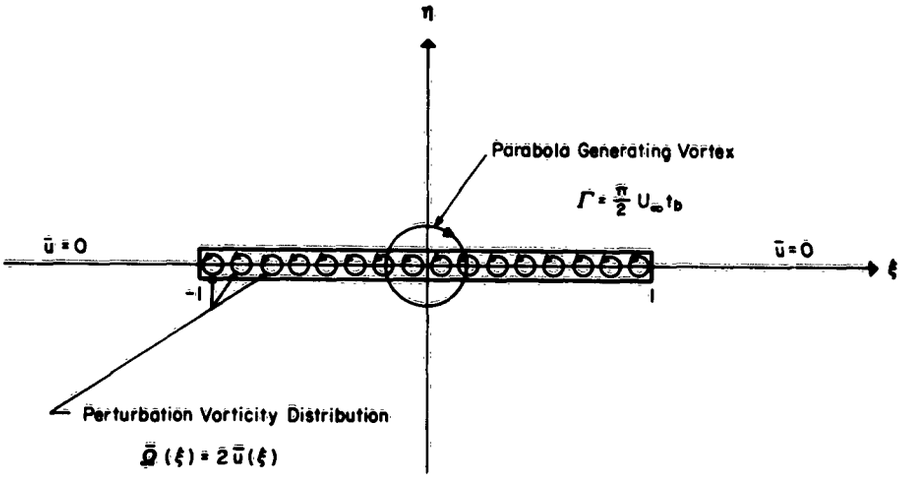

Figure 8- Vorticity Distributions in the Airfoil Plane

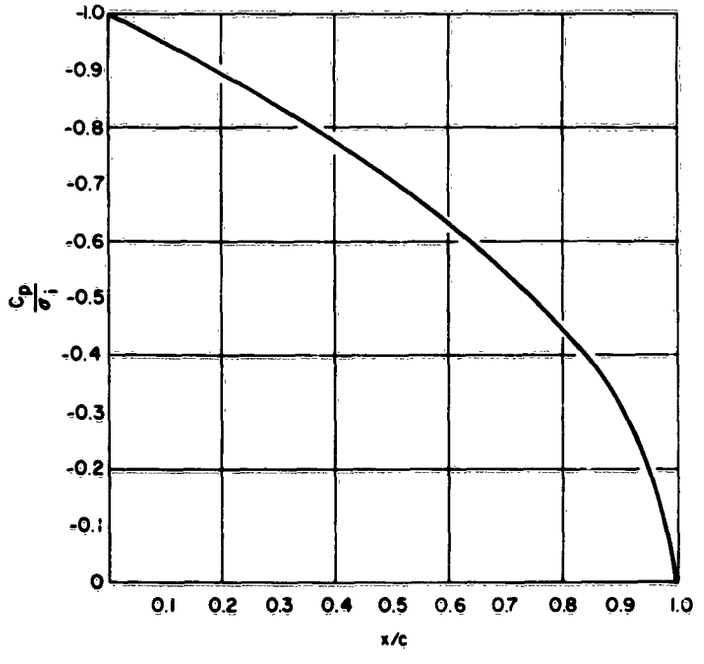

Figure 9- One Term Chordwise Pressure Distribution, $\frac{C_p}{\sigma_i} = -\sqrt{1-x}$

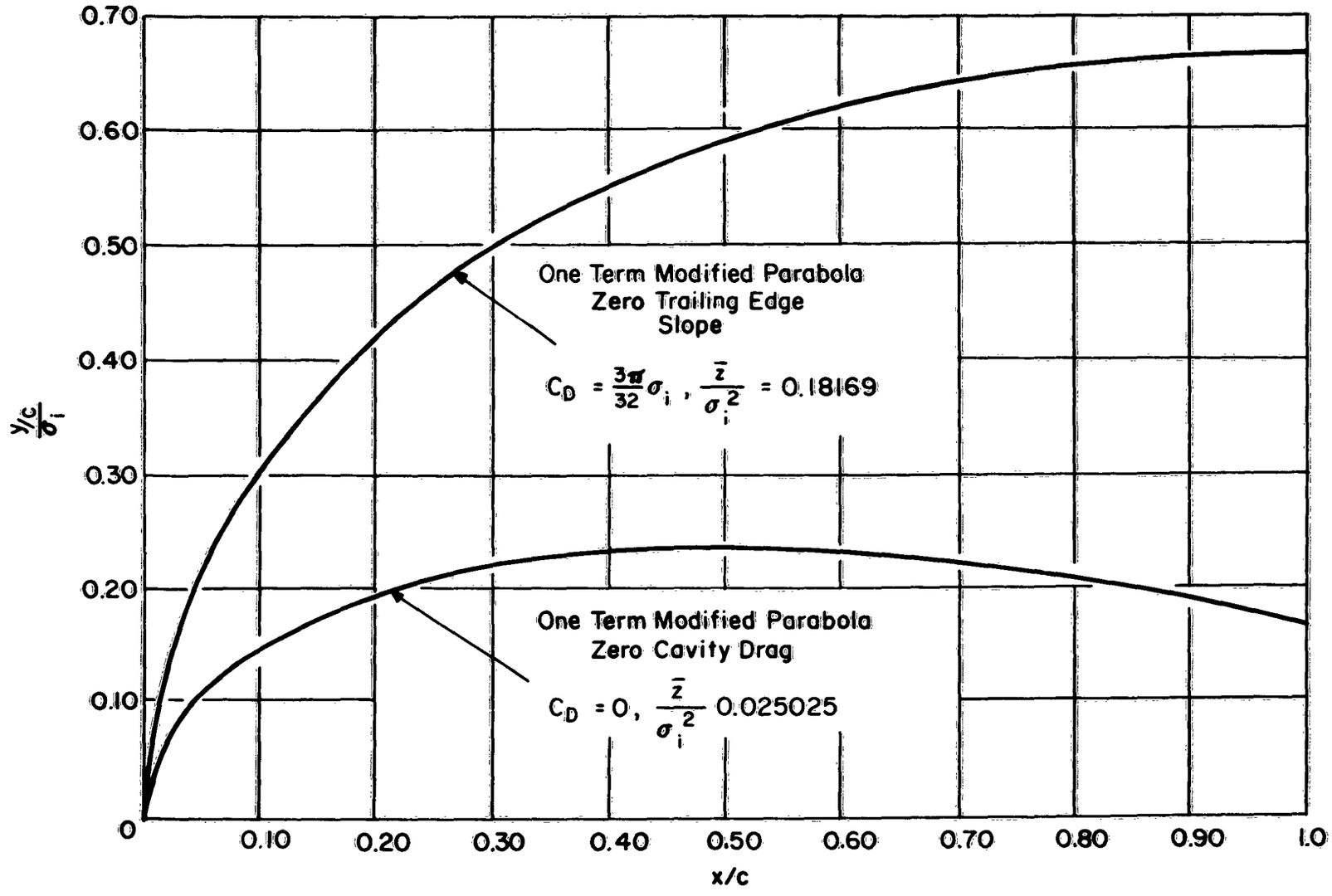

Figure 10- One Term Modified Parabolic Struts

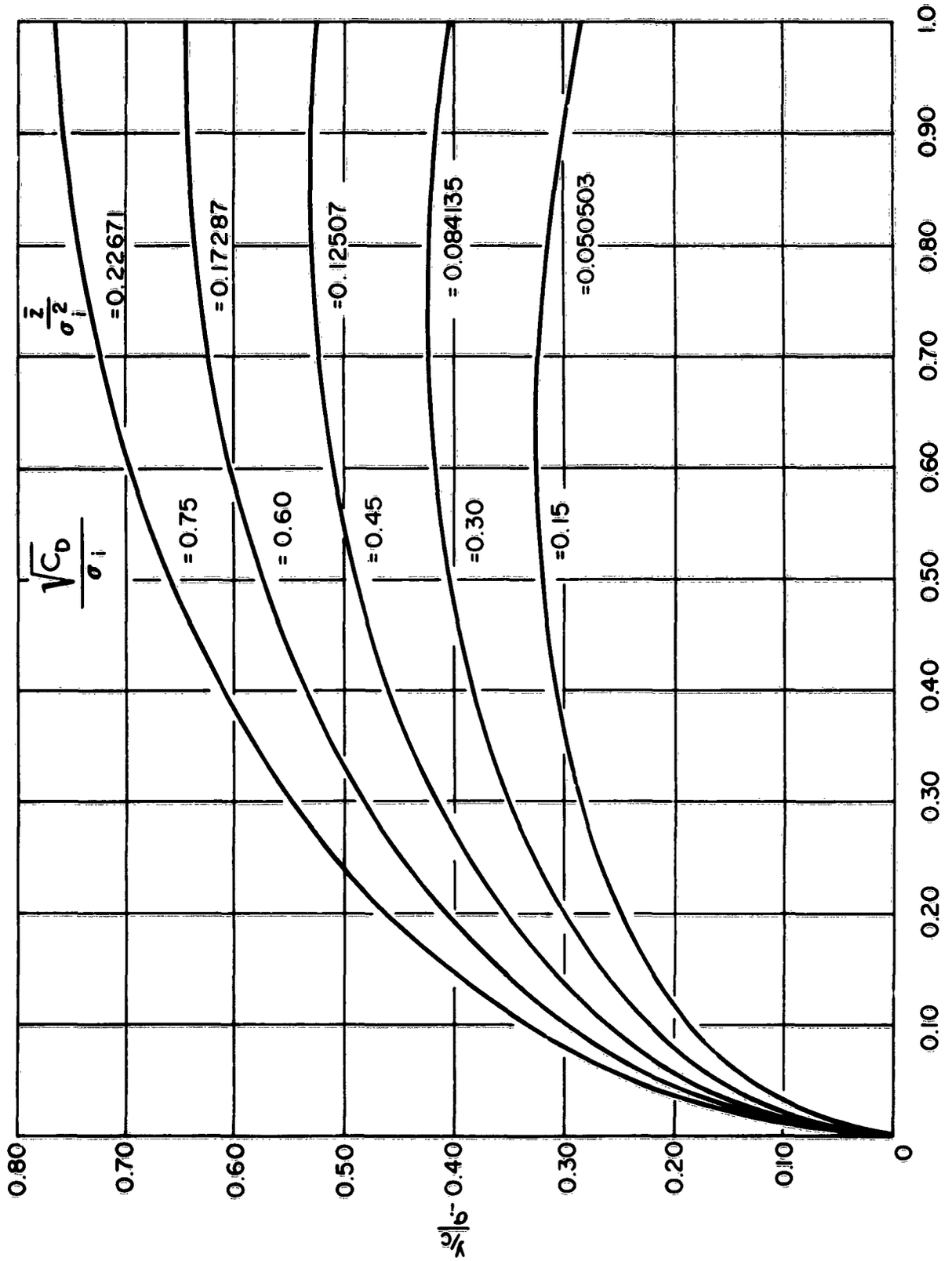

Figure 11- One Term Modified Parabolic Struts with Finite Cavity Drag

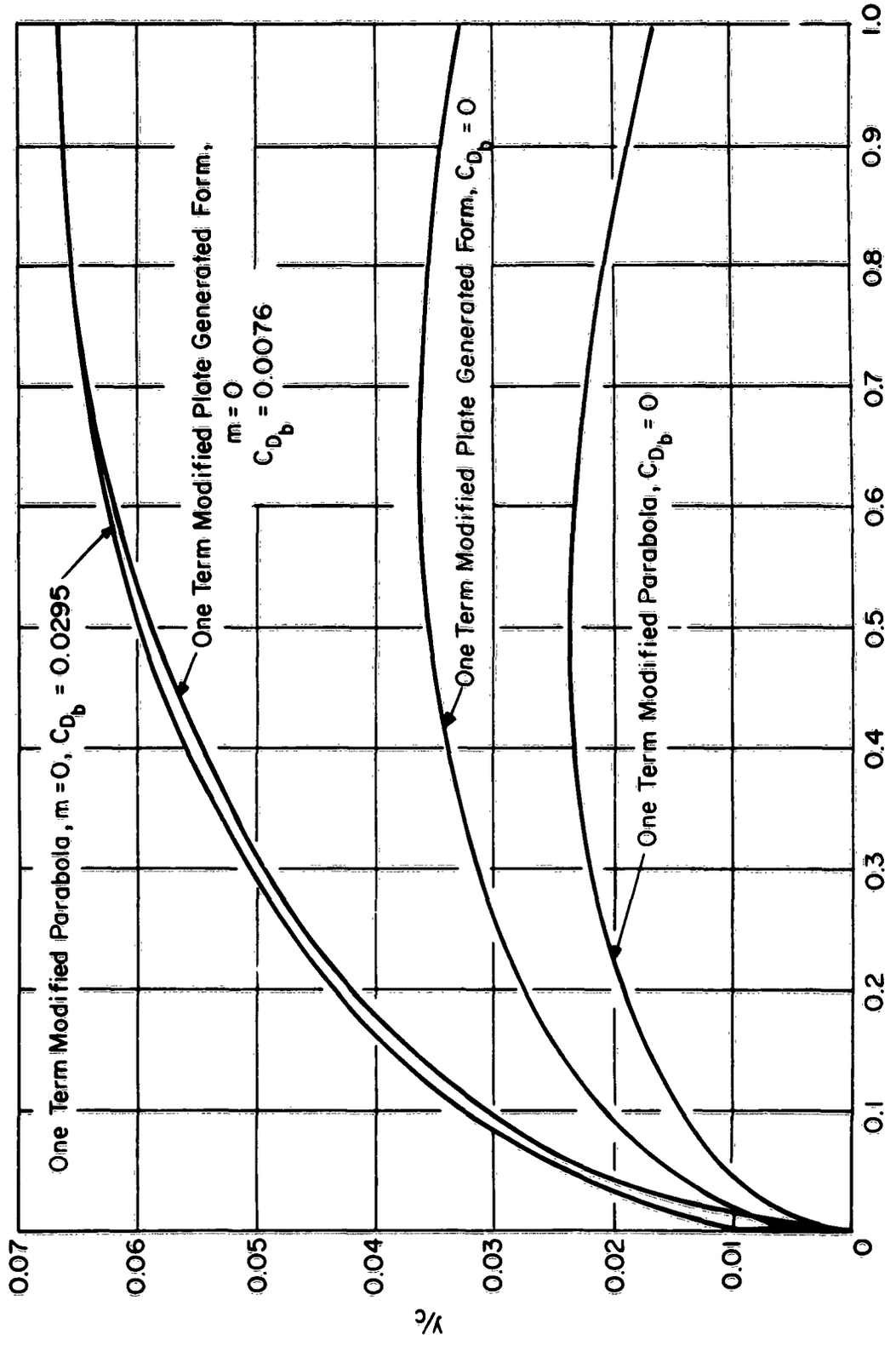

Figure 12 - Comparison of One Term Struts, $\sigma_i = 0.1$

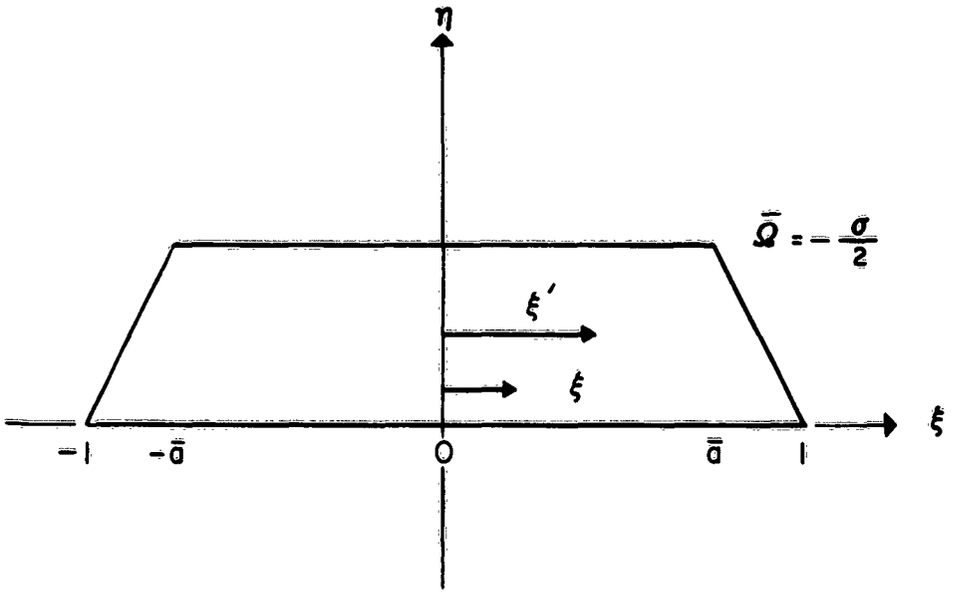

13a- Characteristic Roof Top Vorticity Distribution in Airfoil Plane

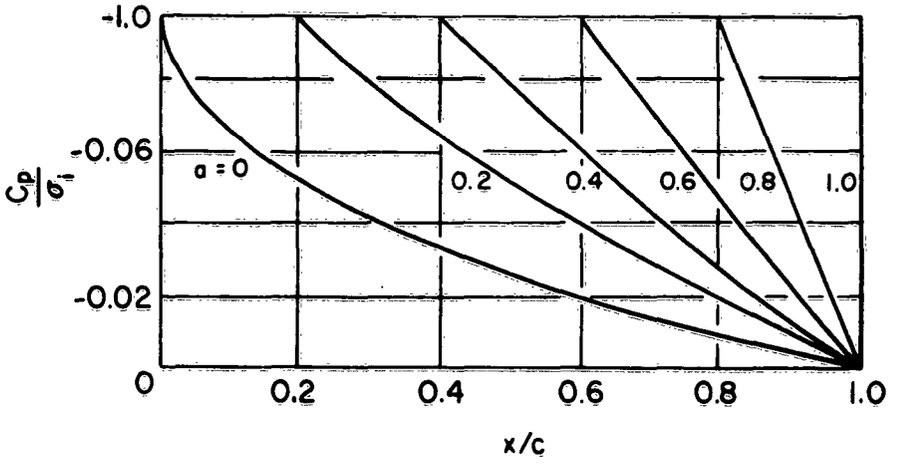

13b-Chordwise Pressure Distribution on Strut

Figure 13- Roof Top Pressure Distributions

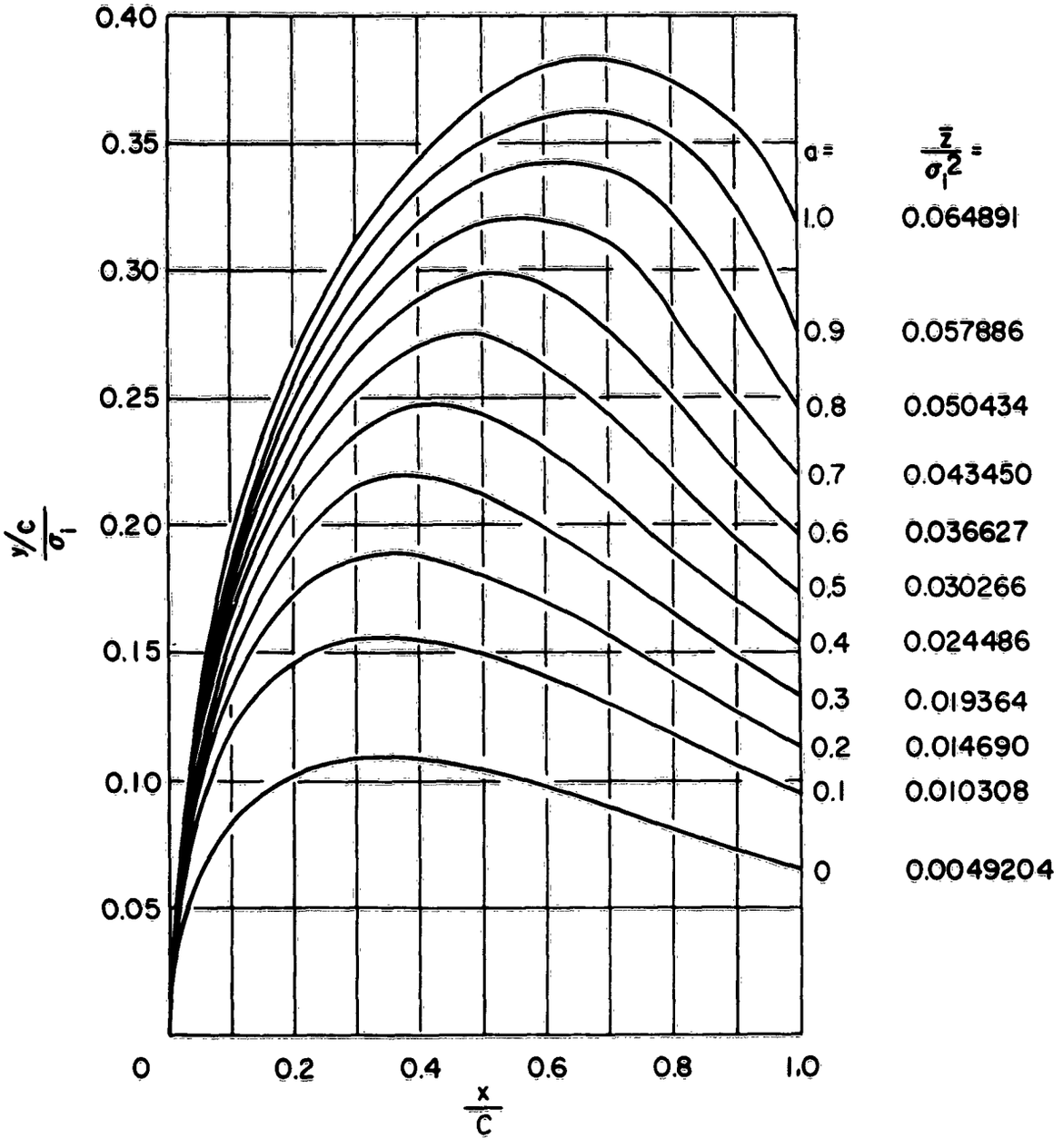

Figure 14- Roof Top Modified Parabolic Struts, Zero Cavity Drag

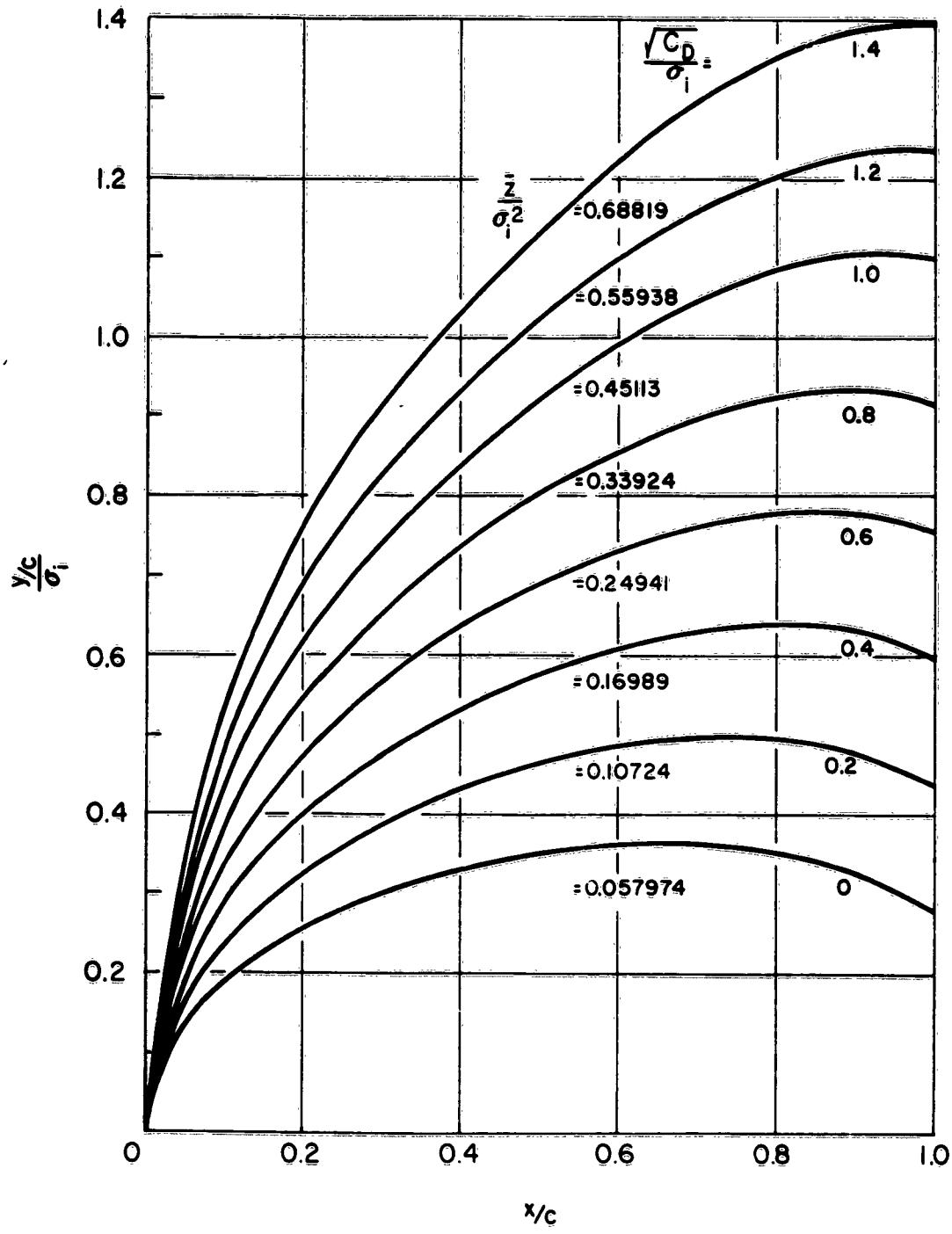

Figure 15 - Roof Top Modified Parabolic Struts With Finite Cavity Drag, $a = 0.9$

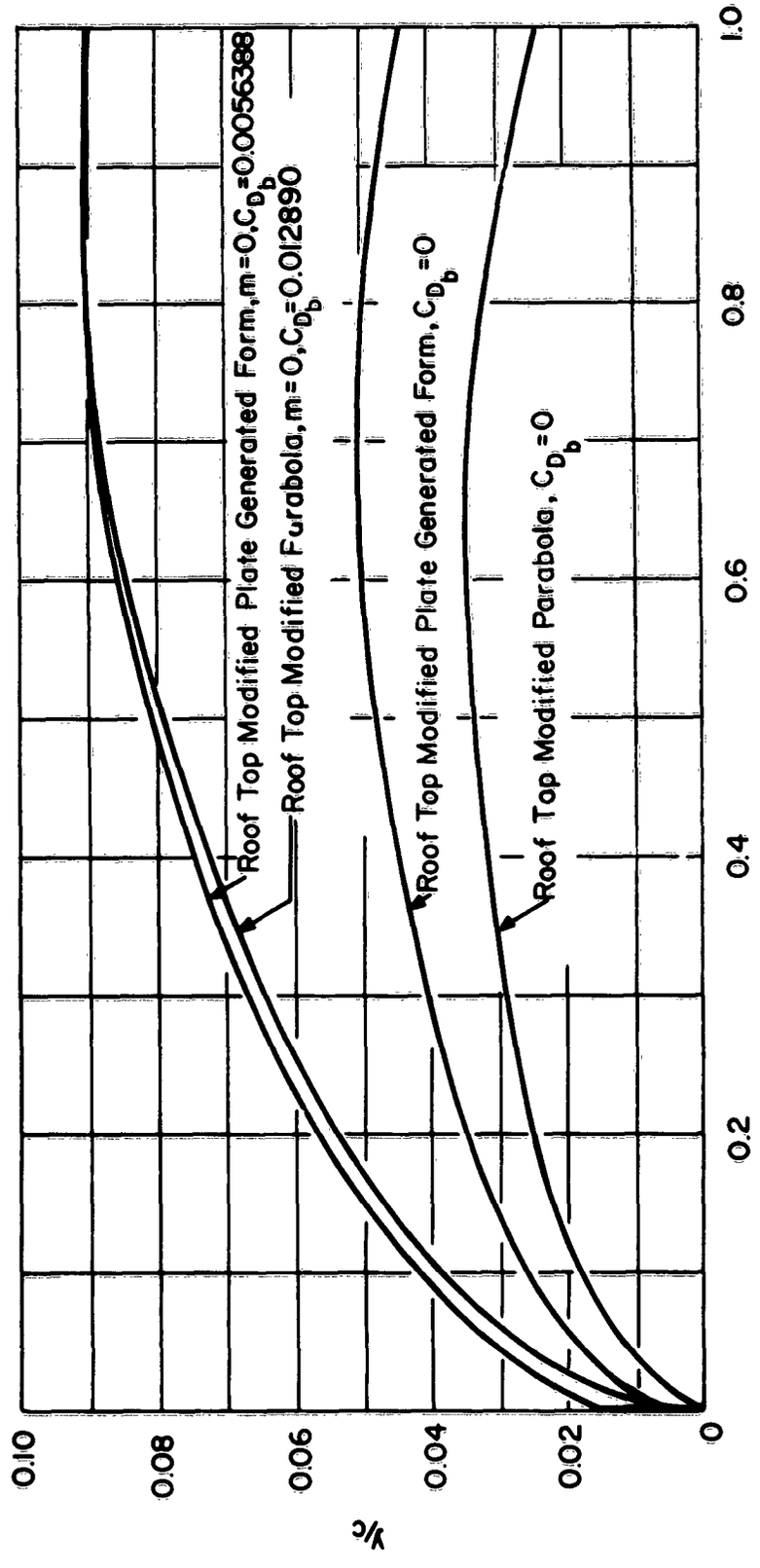

Figure 16- Comparison of Roof Top Struts, a = 0.8, σ=1

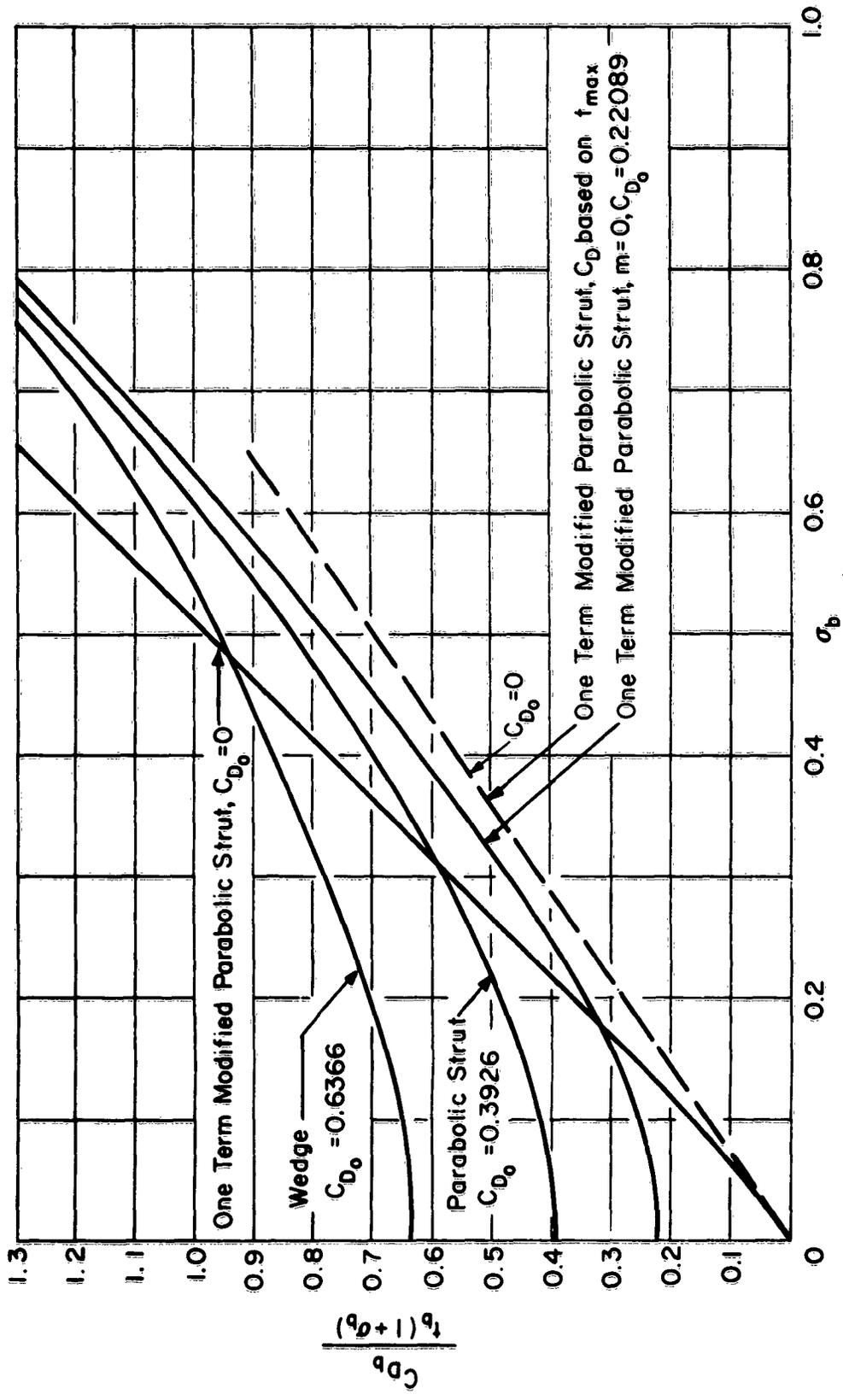

Figure 17- Cavity Drag Coefficient versus Base Cavitation Number for Various Struts

$$C_{D_o} = \frac{C_{D_b}}{t_b(1+\sigma_b)}, \sigma_b = 0$$

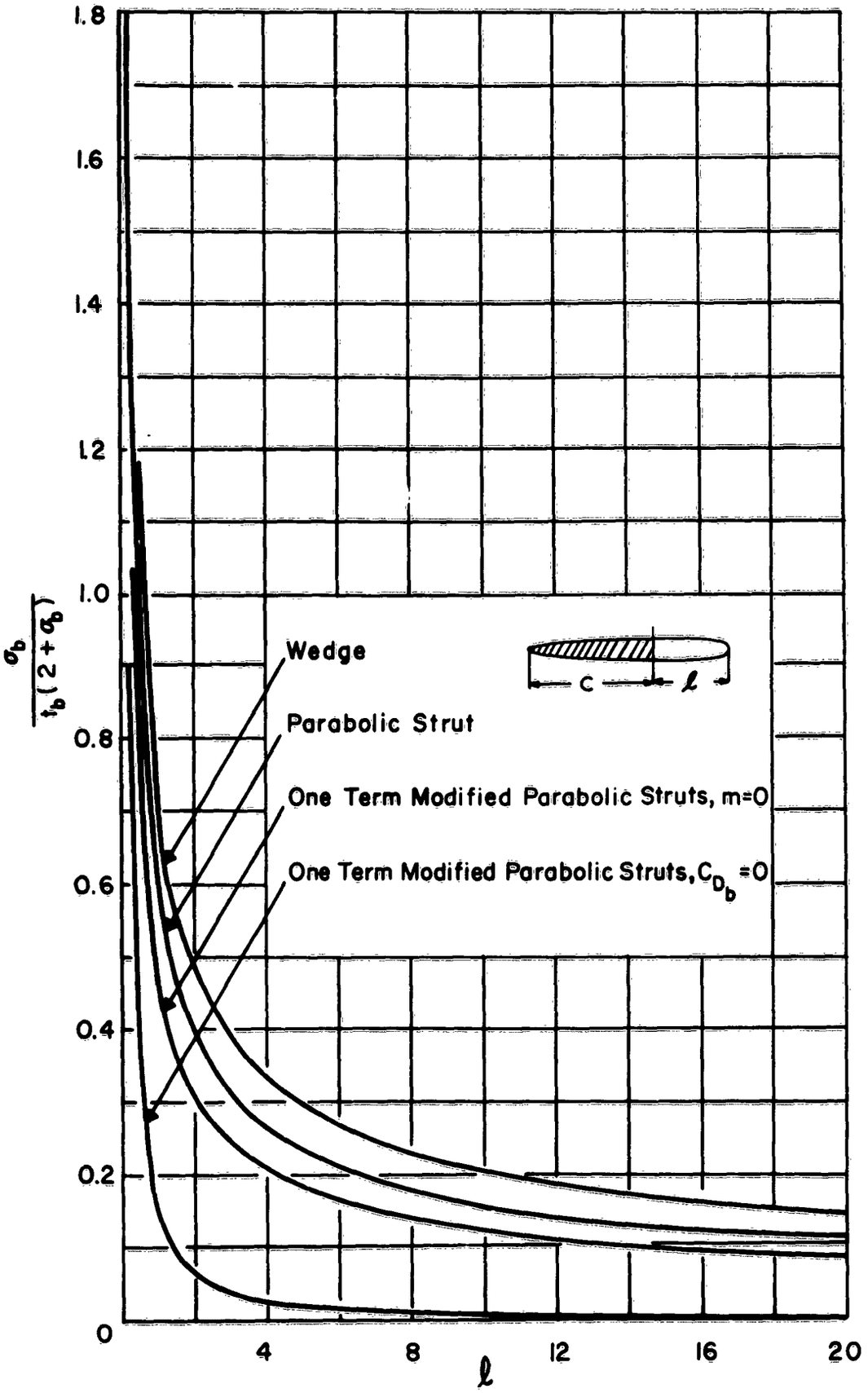

Figure 18 - Cavity Length versus Base Cavitation Number for Various Struts

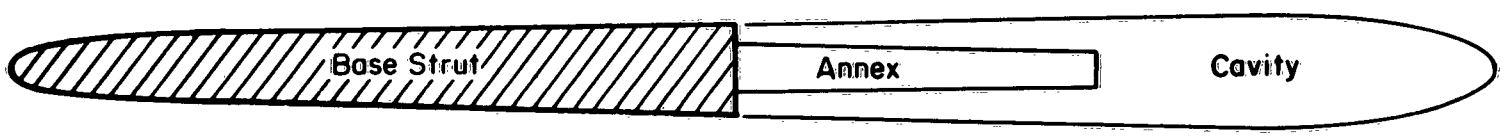

Figure 19- Strut With Base Annex

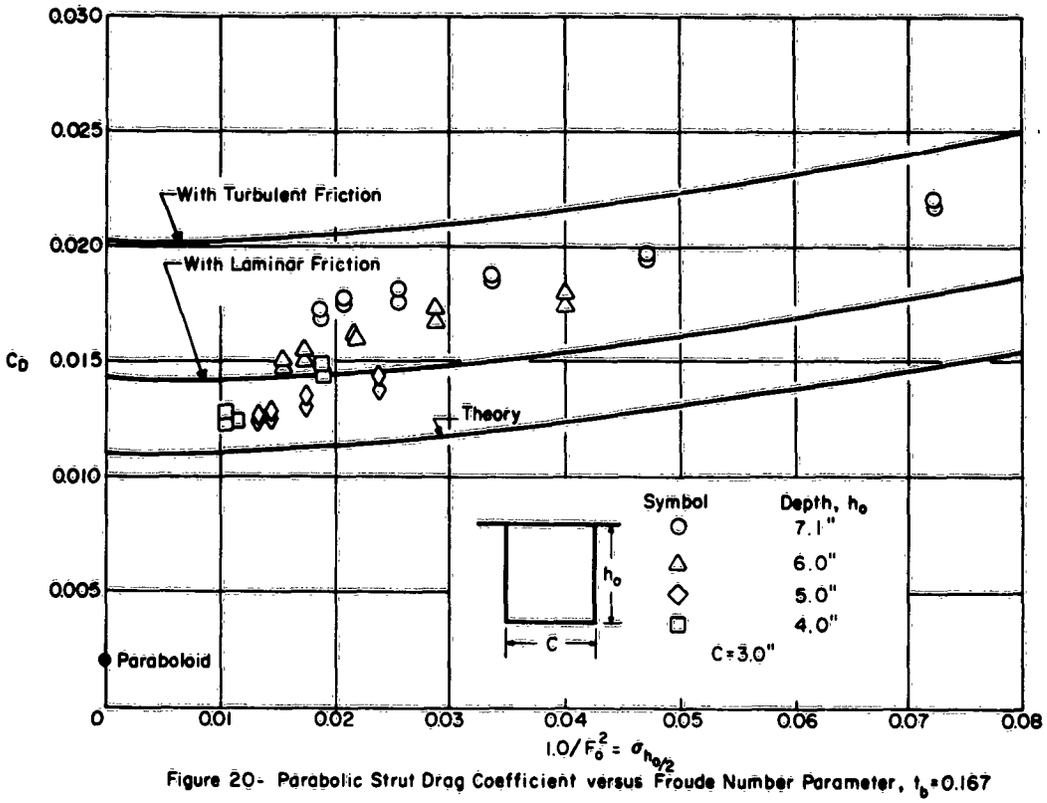

Figure 20- Parabolic Strut Drag Coefficient versus Froude Number Parameter, t_b=0.167

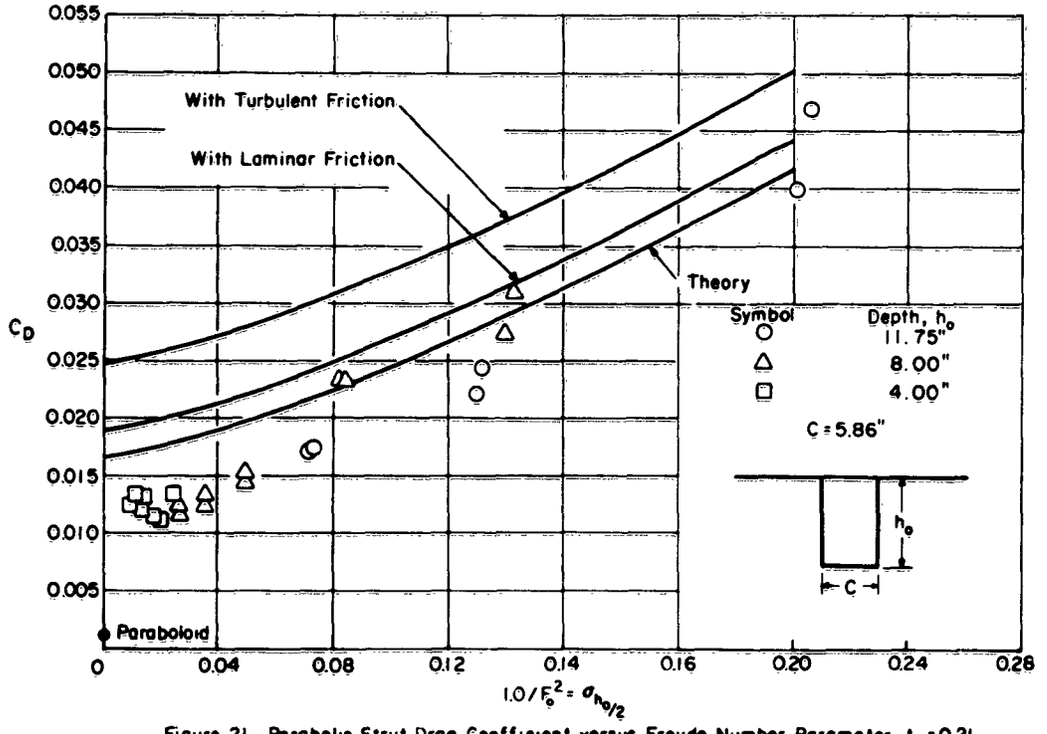

Figure 21- Parabolic Strut Drag Coefficient versus Froude Number Parameter, t_b=0.21

HYDRONAUTICS, Incorporated

DISTRIBUTION LIST

BuShips Contract NObs-78396

		Number of Copies
Chief, Bureau of Ships (60) Navy Department Washington 25, D. C.		
ATTN:	Code 106	1
	Code 335	3
	Code 410	1
	Code 420	53
	Code 442	1
	Code 449	1
Chief, Office of Naval Research (2) Navy Department Washington 25, D. C.		
ATTN:	Code 438	2
Commanding Officer and Director (6) David Taylor Model Basin Carderock, Maryland		
ATTN:	Code 500	1
	Code 513	1
	Code 520	1
	Code 526	1
	Code 530	1
	Code 580	1
Chief, Bureau of Naval Weapons (2) Navy Department Washington 25, D. C.		
ATTN:	Code RAAD-343	1
	Code R-52	1
Commander Armed Services Technical Information Agency Arlington Hall Station Arlington 12, Virginia		
ATTN:	TIPDR	5

HYDRONAUTICS, Incorporated

Mr. John B. Parkinson
Langley Aeronautical Laboratory
National Aeronautics and Space Administration
Langley Field, Virginia 1

Boeing Airplane Company
Aero-Space Division
Box 3707
Seattle 24, Washington 1

California Institute of Technology
Pasadena, California
ATTN: Professor T. Y. Wu
Hydrodynamics Laboratory 1

Convair Hydrodynamic Laboratory
Convair Division
General Dynamics Corporation
San Diego, California 1

Director, Stevens Institute of Technology
Davidson Laboratory
Castle Point Station
Hoboken, New Jersey 1

Grumman Aircraft Engineering Corporation
Marine Engineering Section
Bethpage, Long Island, New York 1

Hughes Aircraft Company
Systems Development Laboratories
Culver City, California
ATTN: Mr. W. N. Turner 1

Hydronautics, Incorporated
200 Monroe Street
Rockville, Maryland 1

The Martin Company
Baltimore 3, Maryland
ATTN: Mr. John D. Pierson 1

Massachusetts Institute of Technology
Department of Naval Architecture and
Marine Engineering
Cambridge 39, Massachusetts 1

Director
University of Minnesota
St. Anthony Falls Hydraulic Laboratory
Hennepin Island
Minneapolis 14, Minnesota 1

Southwest Research Institute
Department of Applied Mechanics
8500 Culebra Road
San Antonio 6, Texas 1

Technical Research Group, Inc.
2 Aerial Way
Syosset, New York 1

Chief of Naval Operations
Navy Department
Washington 25, D. C.
ATTN: Capt. N. H. Fisher, OP-712 1